Max-Planck-Institut
für Meteorologie

REPORT No. 79

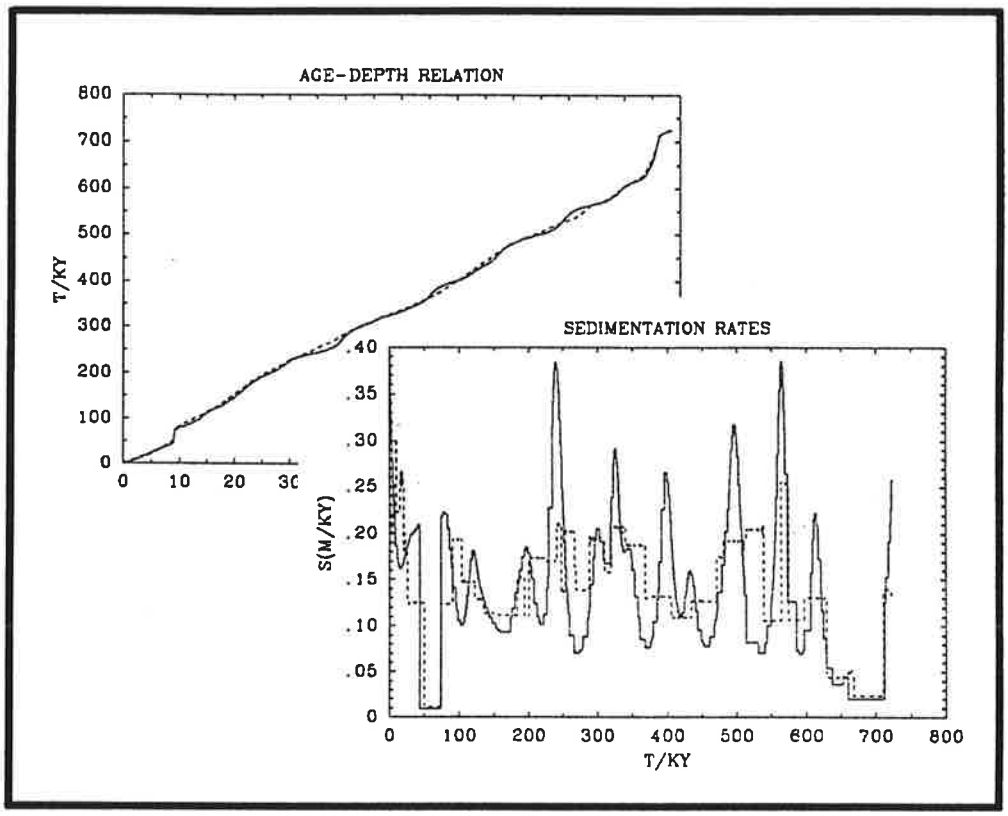

ORBITAL TUNING OF MARINE SEDIMENTARY CORES: AN AUTOMATIC PROCEDURE BASED ON A GENERAL LINEAR MODEL

by

BJÖRN GRIEGER

HAMBURG, JANUARY 1992

AUTHOR:

BJÖRN GRIEGER

MAX-PLANCK-INSTITUT
FÜR METEOROLOGIE

MAX-PLANCK-INSTITUT
FÜR METEOROLOGIE
BUNDESSTRASSE 55
D-2000 HAMBURG 13
F.R. GERMANY

Tel.: +49 (40) 4 11 73-0
Telex: 211092 mpime d
Telemail: MPI.METEOROLOGY
Telefax: +49 (40) 4 11 73-298

REPb79

ISSN 0937–1060

Orbital tuning of marine sedimentary cores: An automatic procedure based on a general linear model

Björn Grieger

Max-Planck-Institut für Meteorologie
Bundesstraße 55, 2000 Hamburg 13, FRG

Abstract

We present a method to optimize the chronology of marine cores by orbital tuning. In a first step—and as an additional result—we calculate a model for the variation of the oxygen isotope abundance ratio throughout the core. The model consists of two components: One results from the convolution of the solar insolation at 65° on July 15 with an impulse response function which is calculated from the data, the other is an additional low-frequency component. The initial age-depth relation of the core can be optimized by minimizing the deviation between model and data. The results of applications on the Meteor core 13519 and the Ocean Drilling Program core site 658 are shown. With the optimized chronologies the model fits the data quite well throughout the investigated cores.

1 Introduction

The aim of this work is to provide a method to obtain the age-depth relation of marine sedimentary cores. The clue are the variations of the solar insolation due to changes of the earth's orbital parameters (inclination between earth axis and orbit plane, relative position of vernal equinox and perihelion, and eccentricity of the orbit).

The *total* insolation which is received by the earth during one year remains always nearly the same—it is not significantly affected by changes in the earth's orbital parameters.[1] Such changes only influence the *distribution* of the insolation in dependence on the latitude and the season. The assumption that variations in this distribution affect the climate—i. e. the global ice volume—is called *Milankovič Theory*. Various suggestions were made which claimed the insolation at a particular season and latitude to be most responsibel for changes in the global ice volume, implicating a certain model of climate interchanges [13]. Most widly used is the insolation at 65°N in summer [9, 11, 12, 20], corresponding to the idea that the annual snow balance mainly depends on summertime melting, and that the growth and decay of the ice sheets is mainly influenced by the annual snow balance at high northern latitudes.

[1]The dependence of the total insolation—integreated over the year and all latitudes—on the eccentricity e is of the order e^2, or 0.1 per cent, and therefore generally considered not to be of any detectable influence on the climate.[5]

Marine sedimentary cores may contain a climatic record provided by the oxygen isotope abundance ratio in the lime shells of micro organisms. The generally used value is

$$\delta^{18}\mathrm{O} := \frac{(n_{18}/n_{16}) - (n_{18}/n_{16})_{\mathrm{today}}}{(n_{18}/n_{16})_{\mathrm{today}}}, \tag{1}$$

where (n_{18}/n_{16}) represents the abundance ratio of the oxygen isotopes $^{18}\mathrm{O}$ and $^{16}\mathrm{O}$. The $\delta^{18}\mathrm{O}$ value in the ocean is a measure of the global ice volume due to fractionation effects of the hydrological cycle. In the evaporation from the sea surface, molecules containing the lighter oxygen isotope $^{16}\mathrm{O}$ are prefered, and so this isotope is stored in increasing ice sheets. This yields an increasing $^{18}\mathrm{O}/^{16}\mathrm{O}$ abundance ratio in the ocean. Micro organisms assimilate the oxygen of their environment, and their lime shells form the marine sediments. Although the isotope abundance in organic sediments may depend on various factors, e. g. the local sea surface temperature and salinity, it is generally believed to reflect essentially the global ice volume [3, 14, 23, 25].

The solar insolation can be calculated for times up to about 10 million years ago with very good accuracy [1, 6, 16, 17], and the hypothesis that the $\delta^{18}\mathrm{O}$ record was influenced by changes in the daily solar insolation on July 15 at 65°N is strongly supported by spectral analysis [8, 9, 10, 13]. The dependence of the $\delta^{18}\mathrm{O}$ record on the solar insolation gives the possibility to obtain information on the age-depth relation of marine cores. Of course it is neccessary to introduce some kind of *a priori* information about the nature of the response. The various models which have been constructed to describe the connection between solar insolation and $\delta^{18}\mathrm{O}$ record differ in the implied *a priori* information.

The most widly accepted Quaternary chronology is the SECMAP time scale due to Imbrie *et al.* (1984), which has a maximum age of nearly 900 ky. It was obtained by manual correlation of the variation of orbital elements—phase shifted corresponding to a simple linear system with an exponential impulse response function and a time constant of 17 ky—with the filtered time series of five cores. After individuell dating the cores were averaged and smoothed to give a standard stack. This can be used to date other cores by stratigraphic correlation.

Herterich and Sarnthein (1984) optimized an age-depth relation for the Meteor core 13519 defined by a polygonian of five points by maximizing the coherence between $\delta^{18}\mathrm{O}$ record and solar insolation, summed over the three astronomical frequency bands (19 ky, 23 ky, and 41 ky).

Martinson *et al.* (1987) developed a time scale back to 300 ky, which was the mean of the results of four different approaches:

- The phases between the dominant components of the orbital forcing and the corresponding components recorded in the data are assumed to be constant.
- The response is assumed to mimic simply the forcing.
- The system function consists of two simple linear models with different time scales for warming and cooling [12].
- The tuning target is constructed from the linear combination of "pure" orbital components and their harmonics.

The final error of the averaged chronology was estimated to be about 5 ky.

Herterich (1988) used a model $\hat{y}$ for the $\delta^{18}O$ variation defined by

$$\frac{d\hat{y}(t)}{dt} = -\lambda\hat{y}(t) + \alpha x(t), \tag{2}$$

where $x(t)$ is the solar insolation, α describes the strength of the forcing, and λ is the inverse time constant of the system. Eq. 2 implies that $\hat{y}$ is obtained from the solar insolation by convolution with an impulse response function of the form

$$h(t) = \begin{cases} \alpha e^{-\lambda t} & \text{for } t \geq 0 \\ 0 & \text{otherwise.} \end{cases} \tag{3}$$

This impulse response function is similar to the one assumed in the development of the SPECMAP time scale, but the time constant of the system was not fixed. The real parameters α and λ and the age-depth relation were calculated by minimizing the deviation between model and data and some further error measures. In this way a time scale of the latest 300 ky was obtained.

In the present paper the impulse response function is not fixed, but is calculated from the data, subject to two conditions securing its physical sence. The formulation of these conditions would be very cumbersome in the frequency domain, and therefore, besides other advantages discussed later, the whole calculation is performed in the time domain, using the method of *regularisation.*

All the models, which are based on the assumption of a linear relation between solar insolation and the $\delta^{18}O$ value, can only reproduce less than about half of the data variance [9, 10, 11, 12, 20]. The reason is, that the $\delta^{18}O$ record is dominated by a 100 ky cycle, a frequency which is not present in the spectrum of the solar insolation. Therefore our model consists of a second portion, an additional low-frequency component, which is requested to be so smooth that it contains no significant power in the astronomical frequency bands.

The construction of a model for the $\delta^{18}O$ variation is one of the two main parts of this work. The other is the optimization of the age-depth relation to minimize the deviation between the estimated model and the $\delta^{18}O$ data. The alternate application of these procedures converges to an optimal chronology and a corresponding model for the $\delta^{18}O$ variation, which fits the data quite well throughout the whole length of the investigated cores, the Meteor core 13519 and the Ocean Drilling Program core site 658.

2 Theory

2.1 The general optimization approach

Every optimization procedure is based on the minimization (or maximization) of a target function, which may be a sum of various components with different weight factors. A general formulation of the target function for the problem at hand under the assumption of a linear relationship between solar insolation and $\delta^{18}O$ value reads

$$\varepsilon = ||WY(f_{\mathrm{ADR}}) - HX||^2 + \alpha\mathcal{A}(H) + \beta\mathcal{B}(f_{\mathrm{ADR}}). \tag{4}$$

Here X and $Y(f_{\mathrm{ADR}})$ are the Fourier transforms of the solar insolation x and the $\delta^{18}O$ value y, respectively, where the argument of Y expresses its dependence on the age-depth

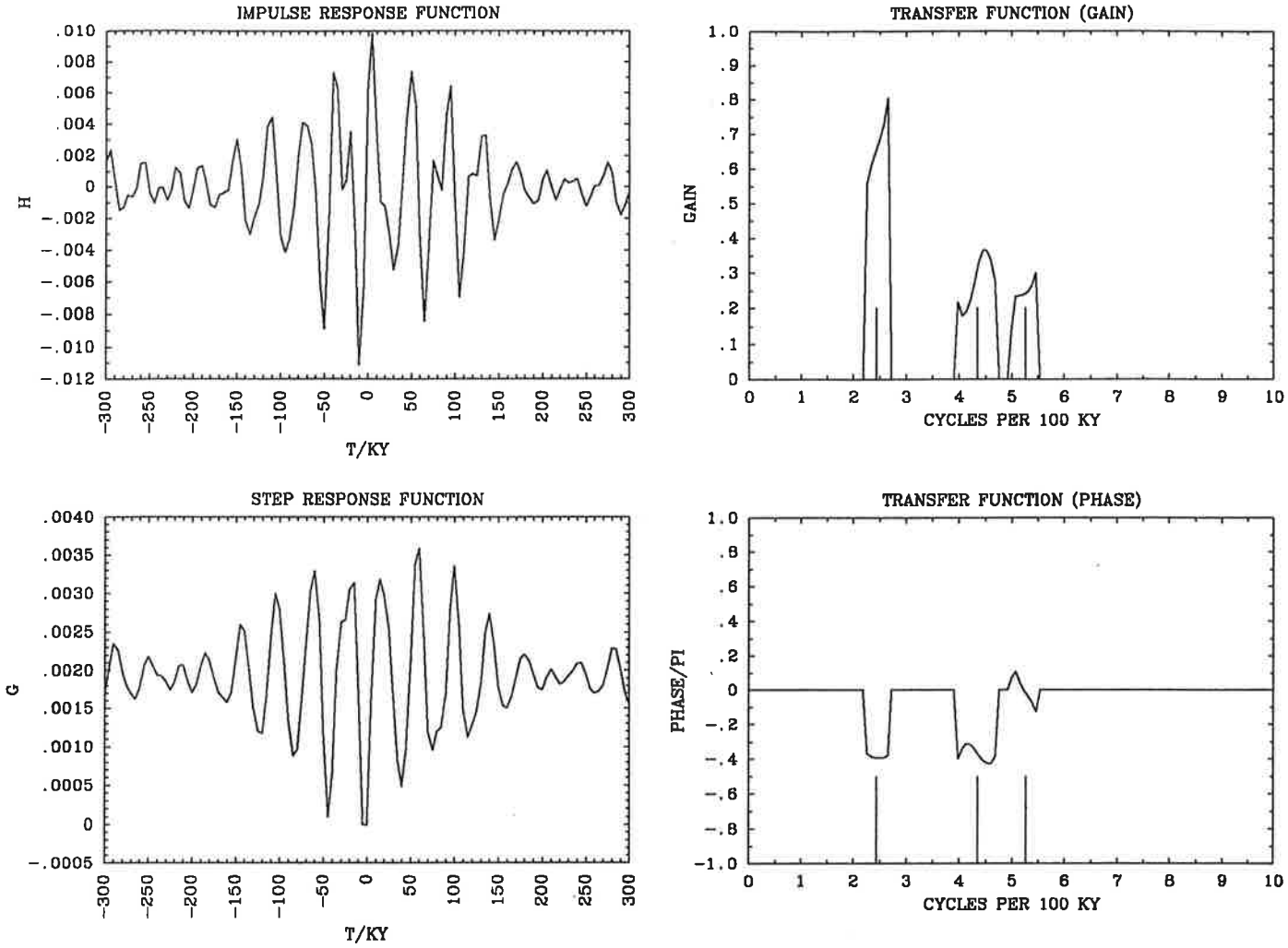

Figure 1: The impulse response function h (upper left), the step response function g (lower left), and gain (upper right) and phase (lower right) of the transfer function H, calculated without any conditions for the Meteor core 13519 in the SPECMAP time scale. Vertical lines indicate the astronomical frequencies (41, 23, and 19 ky).

relation, which is described by the function f_{ADR}. H is the transfer function and W is some window function. The first contribution of the target function can of course also be formulated in the time domain, but the following illustrations are more convenient in the frequency domain. The functions $\mathcal{A}, \mathcal{B} : C^2(\Re, \Re) \to \Re$ attach a "badness" to the transfer function H and the age-depth relation f_{ADR}, while α and β are real weight factors.

First we consider the simple case $W(\omega) = 1$ and $\alpha = 0$. Some claims on the age-depth relation—like smoothness and monotony—in the form of a non-vanishing component $\beta\mathcal{B}(f_{\mathrm{ADR}})$ are necessary to obtain a to some extend reasonable chronology because of the ill-posedness of the problem. Without further conditions the transfer function H can directly be calculated for given x, y, and age-depth relation, but only at the frequencies where the insolation has significant power (appendix A.1). The transfer function for the data of the Meteor core 13519 (section 3.1) in the SPECMAP time scale is shown in Fig. 1, together with its Fourier back transformation, the impulse response function, and the integral of the impulse response function, the step response function. For a physically realizable system the impulse response function has to be zero for negative time, which

is obviously not the case. The step response function, which describes the response of the system to an instantaneous increase of the input at $t = 0$, is also nonsensical. Furthermore, if we try to optimize the age-depth relation—with the method described in section 2.3—it drifts far away from any reasonable chronology without convergence. This indicates that it is necessary to introduce certain conditions on h in form of a badness function $\mathcal{A}(H)$, compare section 2.2.

The model δ^{18}O variation HX can only be non-zero at frequencies where the solar insolation X is also non-zero. This may give rise to the idea to compare the model and the data only at the astronomical frequencies, which implies to filter the data with a frequency window W which is a superposition of three band filters at the astronomical frequencies, i. e. 19, 23, and 41 ky. But time scale optimization of such a target function yields an arrangement of the data that exhibits nearly no power at the astronomical frequencies, which obviously minimizes the deviation between model and data.

However, some filtering of the data is sencefull. The model cannot reproduce the strong 100 ky cycle in the data, and therefore it should be filtered out to prevent the optimization procedure from shifting power from the 100 ky cycle to the astronomical frequencies, which would falsify the resultant chronology. This "filtering" is done by substraction of a low-frequency component which is calculated in one step together with the impulse response function (section 2.2).

In our optimization procedure the minimization is split up into two steps, which are described in the next sections.

2.2 Estimation of a model with given age-depth relation

In this section the calculation of the impulse response function and an additional low-frequency component of the δ^{18}O value is presented. The target function is formulated in the time domain. Besides an easier formulation of claims on the impulse response function this avoids any problems with not equally spaced data.

We proceed from a given age-depth relation. The technique used to calculate a model which describes the response of the δ^{18}O value to changes in the solar insolation is a slightly extended version of the well known *regularisation method* [4, 7, 18, 27]. We assume the model $\hat{y}$ for the δ^{18}O variation y to be given by

$$\hat{y}(t) = \bar{y}(t) + \int_0^\infty h(u)x(t-u)du, \tag{5}$$

where x denotes the daily solar insolation on July 15 at 65°N, h the impulse response function describing the linear impact of x on y, and $\bar{y}$ the low-frequency component of the variation that cannot be explained by a linear model. Eq. (5) can be written in discretized form:

$$\hat{y} = \bar{y} + Xh. \tag{6}$$

Here $\hat{y}$ and $\bar{y}$ are vectors of dimension n, when n is the number of δ^{18}O measurements in the core. We assume the function $h(u)$ to be represented by a polygonian $(u_j, h_j)_{j=1,\ldots,m}$, therefore h is a vector of dimension m and X is an $n \times m$-matrix depending on the solar insolation $x(t)$ and the time coordinates $(u_j)_{j=1,\ldots,m}$ and $(t_i)_{i=1,\ldots,n}$ of h and y, respectively, see appendix A.2. For *physical relizability* h must be zero for negative values of u [15]. This is easily secured because h can only be non-zero between the values of the suplied

$(u_j)_{j=1,\ldots,m}$. For calculations in the frequency domain it would be very cumbersome to obtain physical relizability.

The inverse problem defined by Eq. (6) is ill-posed [4, 7, 18, 27], even if we would omit $\bar{y}$, and to stabilize the solution we have to to introduce some kind of *a priori* information about the unknown functions. Therefore, to find a solution for h and $\bar{y}$, we solve the minimization problem

$$\|y - \bar{y} - Xh\|^2 + \lambda_1 \mathcal{F}(h) + \lambda_2 \mathcal{G}(h) + \mu \mathcal{F}(\bar{y}) = \min, \tag{7}$$

where λ_1, λ_2, and μ are real parameters, and $\mathcal{F}$ and $\mathcal{G}$ are defined to be the discretized equivalent of

$$\mathcal{F} : C^2(\Re, \Re) \to \Re, \quad \mathcal{F}(a) = \int_{t_{\min}}^{t_{\max}} (a''(t))^2 dt \tag{8}$$

$$\mathcal{G} : C^2(\Re, \Re) \to \Re, \quad \mathcal{G}(a) = \int_{t_{\min}}^{t_{\max}} t^2 (a(t))^2 dt. \tag{9}$$

$\mathcal{F}$ attaches to a function the norm of its second derivative and $\mathcal{G}$ attaches the norm of the function itself weighted with t^2, i. e. $\mathcal{F}$ and $\mathcal{G}$ are "badness" functions suppressing solutions which are not smooth or which do not vanish for large t, respectively. The contribution $\lambda_1 \mathcal{F}(h)$ stabilizes the solution of h, i. e. it supresses data noise amplification, whereas beyond that $\mu \mathcal{F}(\bar{y})$ allows $\bar{y}$ to reproduce only the low frequencies of the data.[2] Incorporation of the term $\lambda_2 \mathcal{G}(h)$ secures the *stability* of the system [15].[3] Note that the integral in Eq. (9) represents a multiplication in the time domain which would become a convolution in the frequency domain. Therefore a Fourier transformation of the problem would not result in any simplification.

Derivation of Eq. (7) (see appendix A.4) with respect to the components of h yields

$$(X^T X + \lambda_1 F_1 + \lambda_2 G)h + X^T \bar{y} = X^T y, \tag{10}$$

and derivation with respect to the components of $\bar{y}$ yields

$$Xh + (I + \mu F_2)\bar{y} = y, \tag{11}$$

where F_1 and G are $m \times m$-matrizes and F_2 is an $n \times n$-matrix following from Eqs. (8,9) and the time coordinates of h and $\bar{y}$, respectively, see appendix A.3. I denotes the identity matrix. Eqs. (10,11) represent a system of $(n + m)$ linear equations for the unknown components of h and $\bar{y}$, which has a unique solution, because the matrizes I, F_1, F_2, and G have full rank. The model $\hat{y}$ for the $\delta^{18}O$ variation is then given by Eq. (6).

2.3 Optimization of the age-depth relation for a given model

The optimization of the time scale is a *non-linear* minimization problem. The following formulation provides analytical derivatives of the target funtion and avoids the necessity of any constraints on the variables, which enormously simplifies the iteration procedure.

[2] This is achieved by a suitable choice of the weight factors. The sensitivity of the results is discussed in section 3.3.

[3] Stability is in fact already secured because of the finite range of the time coordinates u of h, but without the additional condition we would obtain an unphysical step at the end of the impulse response function.

Let Δy be definded by

$$\Delta y := y - \bar{y}, \tag{12}$$

i. e. Δy is the residual variation of the data if the low frequency component $\bar{y}$ is substracted (compare section 2.1). Given the solar insolation x and the impulse response function h we can obtain a continous function[4]

$$y_\odot(t) = \int_0^\infty h(u)x(t-u)du, \tag{13}$$

which describes the portion of the $\delta^{18}O$ variation due to changes of the solar insolation. Let $\tau(z)$ be the age-depth relation. Then the deviation between model and data is given by[5]

$$\|y - \hat{y}\|^2 = \sum_{i=1}^{n}[\Delta y_i - y_\odot(\tau(z_i))]^2, \tag{14}$$

where z_i are the corresponding depth coordinates of the $\delta^{18}O$ values y_i in the core.

The function we optimize is the *inverse* sedimentation rate $r(z)$. This choice has several advantages, as we shall see below. The age-depth relation is expressed through r by

$$\tau(z) = \int_0^z r(z')dz'. \tag{15}$$

In the discretized formulation we assume $r(z)$ to have the constant value r_i between neighbouring depth coordinates z_{i-1} and z_i. The corresponding time coordinates are given by

$$\tau(z_i) = \sum_{j=1}^{i} r_j \cdot (z_j - z_{j-1}), \tag{16}$$

with $z_0 := 0$.

To avoid excessive oscillation[6] of the sedimentation rate $s_i = 1/r_i$ we add the norm of the second derivative of s to the deviation given by Eq. (14). So we obtain the target function

$$\varepsilon(r) := \sum_{i=1}^{n}[\Delta y_i - y_\odot(\tau(z_i))]^2 + \lambda\mathcal{F}(s), \tag{17}$$

where $\mathcal{F}$ is defined by Eq. (8). Note that τ and s depend on r. The derivatives $\partial\varepsilon/\partial r_j$ can be calculated (see appendix A.5) and ε can be minimized using standard minimization techniques. Our results were obtained with the conjugate gradient method due to Fletcher and Reeves. Finally the new time coordinates $(t'_i)_{i=1,\ldots,n}$ of the depth coordinates $(z_i)_{i=1,\ldots,n}$ are given by

$$t'_i = \tau(z_i). \tag{18}$$

If a variable r_i becomes large during the iteration, the sedimentation rate s_i tends to zero, but cannot become negative. If, on the other hand, r_i approaches zero, the sedimentation rate tends to infinity, which is prohibited by the increasing badness $\lambda f(s)$, and in this case r_i and s_i can also not become negative. Therefore the monotony of the age-depth relation is secured without further constraints on the variables.

[4]We can treat $y_\odot$ as a continues function because h and x can be calculated with arbitrary high resolution, so that reasonable interpolation is possible.

[5]For ilucidation note that in the trivial case $\tau(z_i) = t_i$ (i. e. $\tau(z)$ represents the initial age-depth relation which was used to calculate h and $\bar{y}$) the right side of Eq. (14) becomes $\|\Delta y - Xh\|^2$.

[6]I. e. to stabilize the solution of the ill-posed problem.

If there are hiatuses in the core, the true sedimentation rate is not smooth at the points where the hiatuses occur. Because we require smoothness of the sedimentation rate in Eq. (17), the solution would be a poor representation of the true sedimentation rate. This problem can be accounted for very simply: If we presume a hiatus between the depth coordinates z_{i-1} and z_i, the point s_i has to be omited in the calculation of the badness $\lambda\mathcal{F}(s)$ in Eq. (17). So s_i can differ from its neighbouring values without punishment, especially it can tend to zero.

Note that any calculation in the frequency domain would require to optimize the inverse function $z(t)$, because equally spaced time coordinates are needed. Therefore the *time* coordinates of a hiatus would have to be fixed *a priori*, while our method only requires the *depth* coordinates and allows the time coordinates to be adjusted by the optimization procedure to reconcile model and data.

2.4 Iterative optimization of response model and age-depth relation

The input data required for the estimation of an age-depth relation and the corresponding response model are:

- The δ^{18}O values $(y_i)_{i=1,\dots,n}$ in the core,
- the corresponding depth coordinates $(z_i)_{i=1,\dots,n}$,
- an initial guess for the time coordinates $(t_i)_{i=1,\dots,n}$.

Application of the procedure described in section 2.2—which mainly consists of the solution of a linear equation system—yields a model $\hat{y}$ for the δ^{18}O variation and hence a deviation between this model and the data y. It is not advisable to minimize the deviation $\|y-\hat{y}\|^2$ iteratively by calculating a new model for each new age-depth relation, because the calculation of a model takes much time and the derivatives of $\|y-\hat{y}\|^2$ with respect to the age-depth relation parameters r_j cannot be calculated due to the implicit dependence of $\hat{y}$ on the age-depth relation. So the iteration would be very cumbersome.

Instead we keep the model fixed and optimize the time coordinates of the data using a standard minimization technique, as described in section 2.3. So we obtain a new age-depth relation, which minimizes the deviation between the data and the fixed model. Using the new time coordinates we can calculate a new model, and so on.

During these iterations the parameters λ_1 and λ_2 for the response model estimation, compare Eq. (7), remain fixed. On the contrary the parameter μ has to be adjusted according to changes in the total length of the time series due to optimization of the age-depth relation for the following reason: If the time scale of a time series is expanded by a factor a, the norm of the second derivative, see Eq. (8), decreases by a factor a^{-3}. This would allow $\bar{y}$ to become less smoother and lead to minimization of the deviation $\|y-\hat{y}\|^2$ just by expansion of the whole time series. Therefore μ has to be scaled proportional to ΔT^3 for each new response model estimation, when ΔT is the new total length of the series.

The alternate model estimations and time scale optimizations are repeated until the age-depth relation does not change anymore. In some cases it may be necessary to average

over successive iterations to achieve convergence. That means we introduce a damping paramerer γ with $0 < \gamma < 1$ and obtain the new time coordinates from

$$t_i' = (1 - \gamma)t_i + \gamma\tau(z_i), \tag{19}$$

where t_i are the initial time coordinates of the depth coordinates z_i and $\tau(z)$ is the new estimated age-depth relation. An alternative approach to introduce a kind of damping is to terminate the time scale optimization and switch to the model calculation *before* the solution with minimum deviation is reached. This strategy may yield some calculation time saving provided that the minimization algorithm behaves reasonable.

3 Applications and results

3.1 Meteor core 13519

The Meteor core 13529 was taken from the Sierra Leone Rise at 5°N, 20°W in the equatorial Atlantic, position of DSDP site 366, in 2862 m water depth. It is 10.67 m long and the maximum age exceeds 750 ky. The δ^{18}O curve (see Fig. 2) was obtained from the planktonic species *Globigerinoides sacculifer*. It consists of 179 data points, which corresponds to a mean sampling intervall of about 4 ky.

For the optimization procedure an initial time scale is needed. Various experiments show that a simple linear age-depth relation, assuming a constant sedimentation rate over the hole core, is not of sufficient accuracy. In some regions of the core the attached initial age would be very far from the "true" age (which we assume to be somewhat near the SPECMAP age), and the optimization procedure is not able to shift it across some intermediate insolation extrema. Therefore we use the depth coordinates of the boundaries of the isotopic stages 1–20 [22], as given by Sarnthein *et al.* (1984), to fix the initial age-depth relation. To these points we attach the ages given by the SPECMAP time scale [14]. The initial chronology is then obtained by linear interpolation.

The δ^{18}O variation in the resultant time scale and the corresponding model—calculated as describes in section 2.2—are shown in Fig. 2. As described in section 2.2 the model consists of two components: the sun-induced variations $y_\odot$ and the intrinsic low-frequency variations $\bar{y}$, which are also shown in Fig. 2. Due to the unconvenient initial age-depth relation $y_\odot$ is small compared with $\bar{y}$, i. e. with this age-depth relation only a small fraction of the δ^{18}O variation can be explained by linear impact of the solar insolation. The other model component, $\bar{y}$, can only reproduce the low-frequency features of the data. The data variance explained by the two model components is compared in table 2.

During the optimization procedure the age-depth relation is adjusted to allow a larger response to solar insolation, which is reflected in an increase of $y_\odot$ (see Fig. 4), and a decrease of the mean deviation between model and data from 0.31 to 0.27. The variance explained by $y_\odot$ is considerably increased while the variance exlained by the intrinsic low-frequency component $\bar{y}$ is slightly decreased, compare table 2. The resultant age-depth relation and the corresponding sedimentation rates are shown in Fig. 3. A comparison between the δ^{18}O data before and after the time scale optimization and their agreement with the optimized model is shown in Fig. 4, together with the two components of the model. The increased $y_\odot$ is also reflected in the impulse response, the step response, and

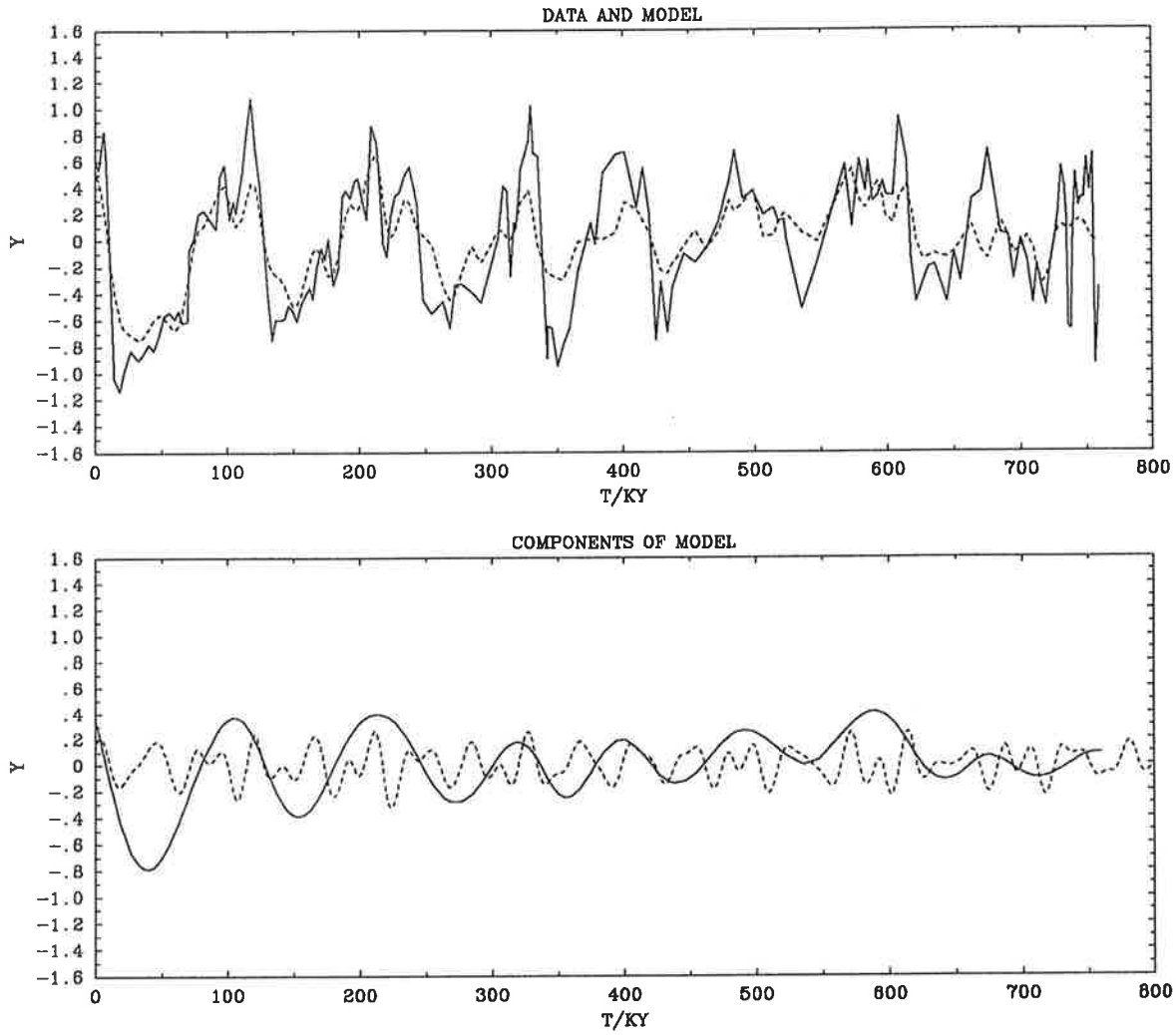

Figure 2: Meteor core 13519, SPECMAP age-depth relation. *Top:* The δ^{18}O variation (solid line) and the model (dashed line). *Bottom:* The two components $\bar{y}$ (solid line) and $y_{\odot}$ (dashed line) of the model.

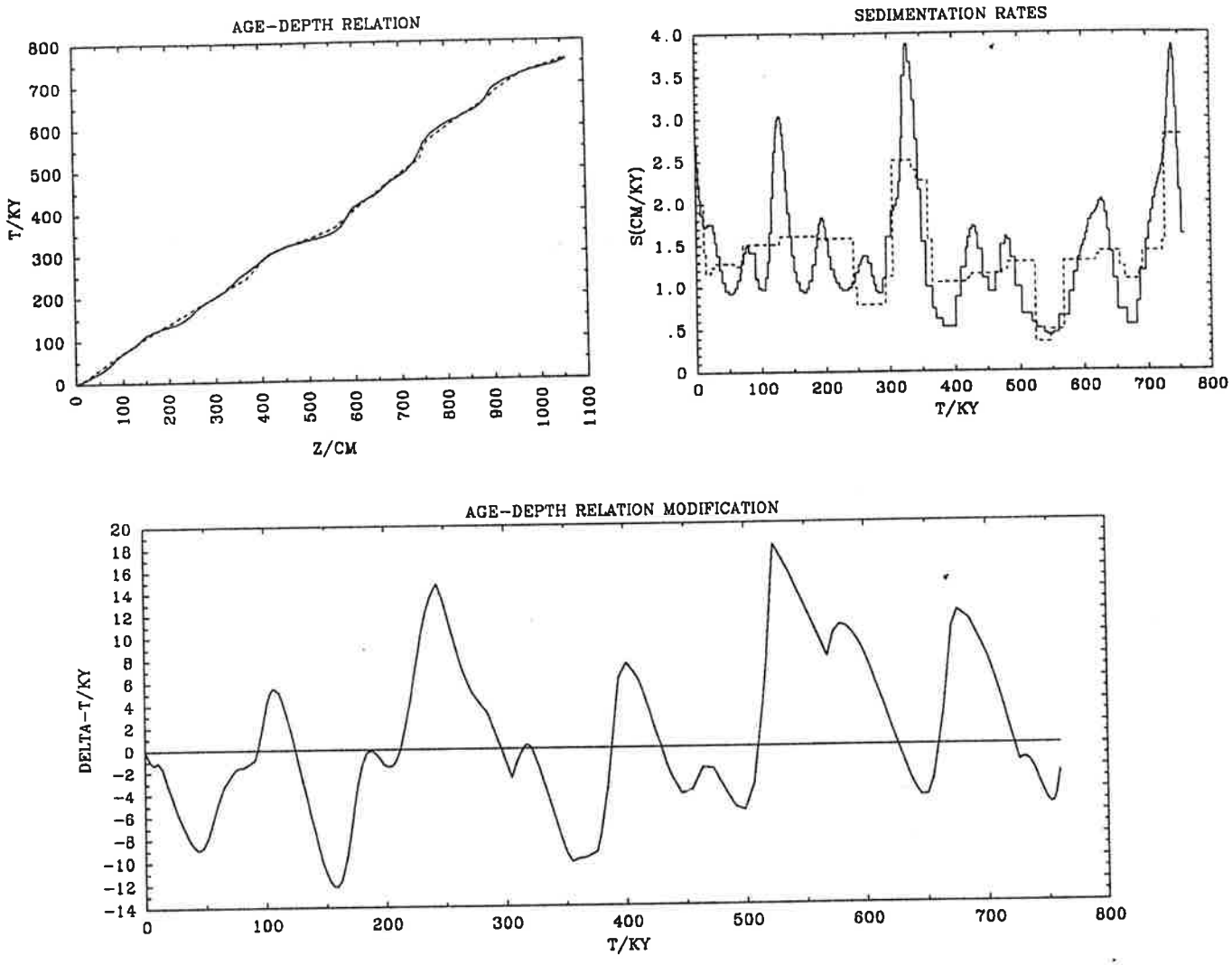

Figure 3: Meteor core 13519. *Top left:* The initial (dashed) and optimized (solid) age-depth relation. *Top right:* The initial (dashed) and optimized (solid) sedimentation rate. *Bottom:* The difference of the optimized and the initial age-depth relation. The mean deviation is 6.5 ky.

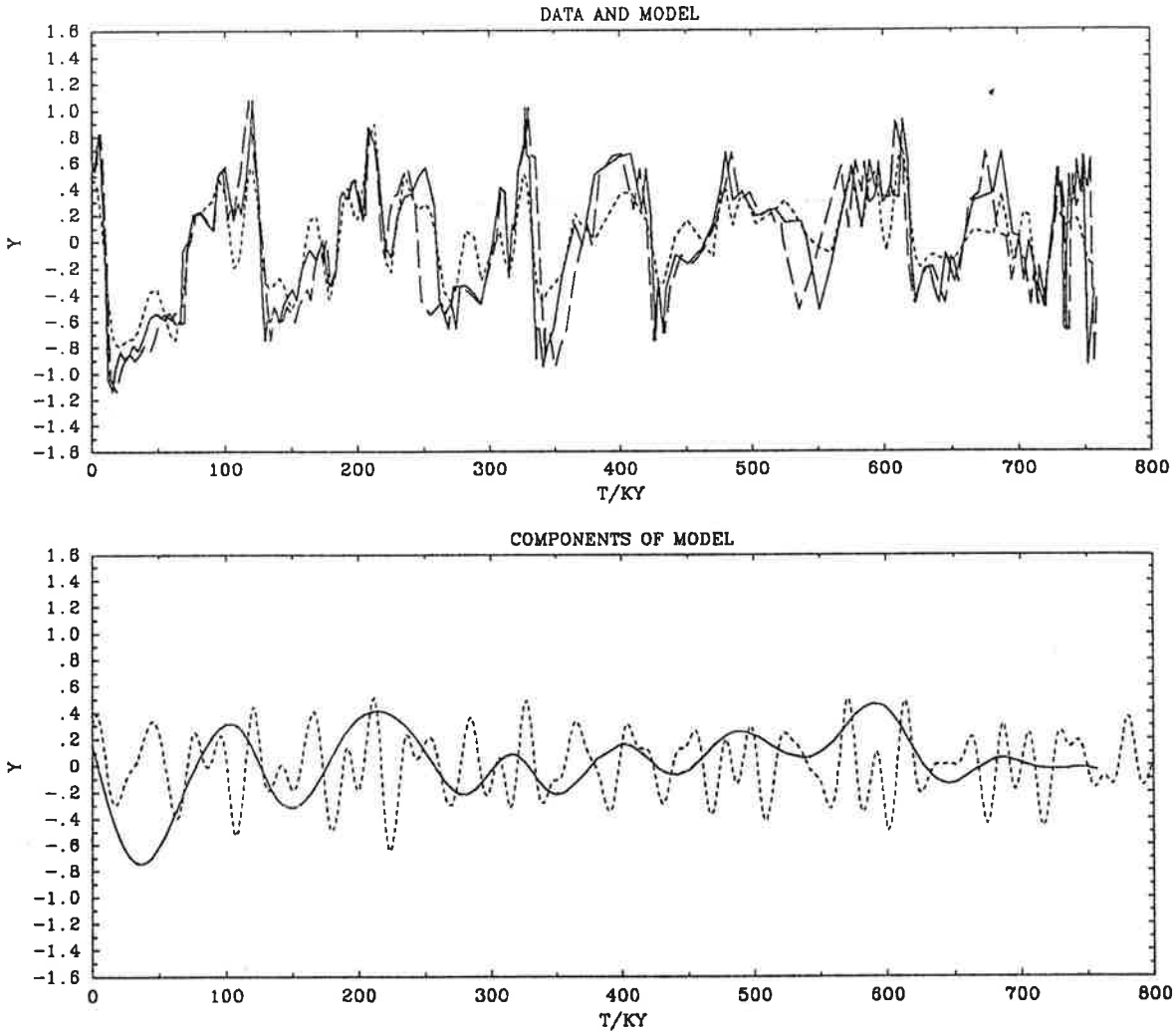

Figure 4: Meteor core 13519. *Top:* The $\delta^{18}O$ variation in the initial (long dashed) and in the optimized time scale (solid line), and the model for the optimized time scale (short dashed). *Bottom:* The two components $\bar{y}$ (solid line) and $y_{\odot}$ (dashed line) of the model.

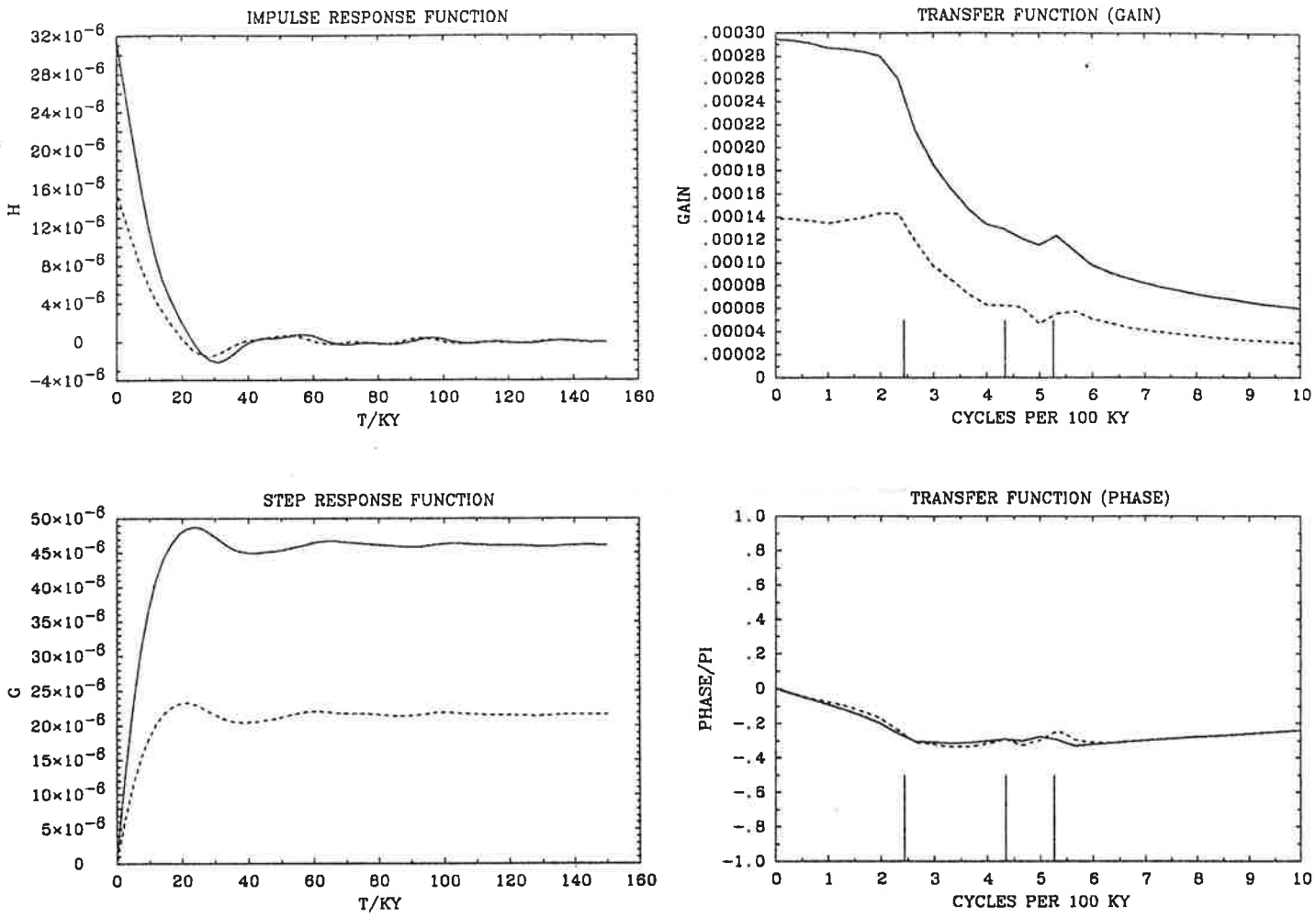

Figure 5: Meteor core 13519: The impulse response function h (upper left), the step response function g (lower left), and gain (upper right) and phase (lower right) of the transfer function for the initial (dashed line) and the optimized (solid line) age-depth relation. Vertical lines indicate the astronomical frequencies (41, 23, and 19 ky).

the transfer function[7], which are shown in Fig. 5.

The coherency between the solar insolation and the $\delta^{18}O$ variation in the initial and the optimized time scale is presented in Fig. 6. For the initial time scale peaks can be recognized in the astronomical frequency bands, but the coherency is quite small at the 95 per cent confidence level. Due to the optimization the squared coherency in the 41, the 23, and the 19 ky band increases to 80, 60, and 50 per cent, respectively. Therefore the examination of the coherency spectra confirms that the time scale optimization procedure considerably increases the linear correlation of the solar insolation and the $\delta^{18}O$ record.

The Brunhes-Matuyama magnetic reversal was determined to be at a depth between 981 and 989 cm [2]. With our resultant chronology this implies an age between 729 and 732 ky.

[7]The step response and the transfer function are not incorporated in the optimization procedure. They are just shown for illustration.

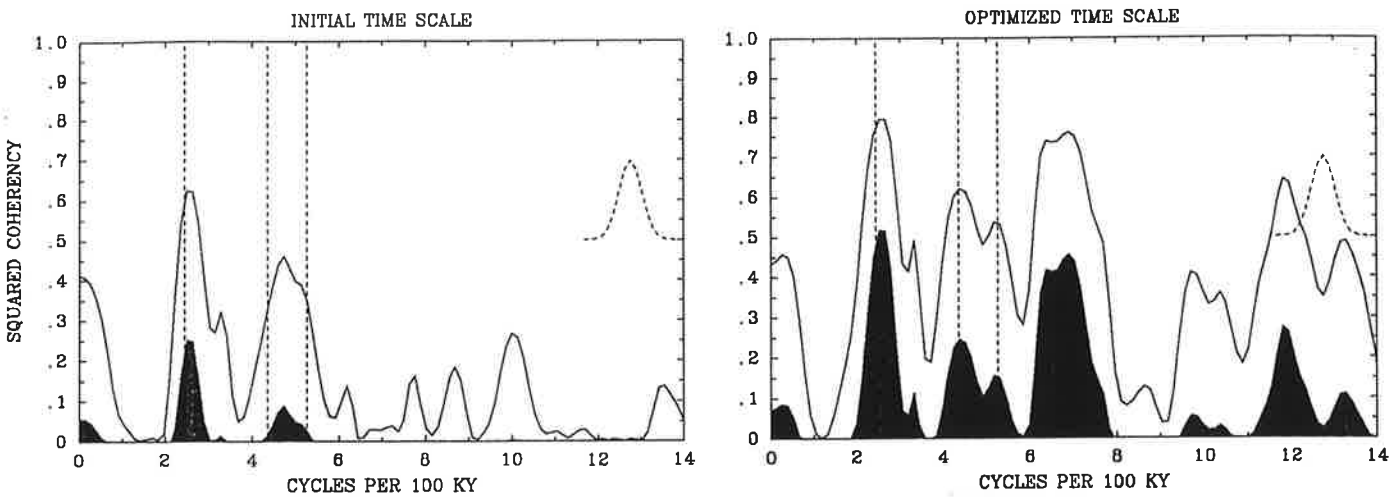

Figure 6: Meteor core 13519: Squared coherency between insolation and δ^{18}O data in the initial (left) and the optimized time scale (right). Shaded regions denote the lower 95 per cent confidence limits. Vertical dashed lines indicate the astronomical frequencies (41, 23, and 19 ky). Dashed curves at the right margin display the spectral window.

3.2 The Ocean Drilling Program core site 658

The core ODP 658 off north-west Africa is nearly 100 m long and the maximum age of the used δ^{18}O data is about 730 ky. The large sedimentation rates enable an extraordinary high resolution with measurements at 382 depth coordinates, which corresponds to a mean sampling intervall smaller than 2 ky. We use the δ^{18}O data estimated from the benthic species *Cibicidoides wuellerstorfi* [26].

The initial age-depth relation we use was estimated by Sarnthein and Tiedemann (1990) according to the SPECMAP time scale [14]. There are two hiatuses at $z = 9$ m and $z = 96$ m, which we take into account in the way described in section 2.3.

The δ^{18}O variation in the initial time scale and the corresponding model are shown in Fig. 7. The fit between model and data is quite better than for the Meteor core 13519 in the initial time scale, and the two components $y_\odot$ and $\bar{y}$ of the model, see Fig. 7 (compare section 2.2), are of the same order of magnitude. The variance explained by the model is quite larger than for the Meteor core 13519 for the initial time scale, see table 2. This may in part be due to the fact that almost every isotopic stage was dated according to the SPECMAP time scale, whereas for the meteor core the initial age-depth relation was obtained by linear interpolation of only the boundaries of the major stages 2–20 because of the lower resolution.

Nevertheless the optimization procedure leads to further improvement. The resultant age-depth relation and the corresponding sedimentation rates—compared with the initial values—are shown in Fig. 8. During the optimization the mean deviation between model and data decreased from 0.28 to 0.24. Fig. 9 shows the δ^{18}O data and the model in the optimized time scale, and for comparison the δ^{18}O data before the time scale optimization. Also shown are the two components of the model. Note that the model component $y_\odot$ is increased due to the optimization, likewise the the impulse response, the step response, and the transfer function, which are shown in Fig. 10.

The total explained variance is considerably larger for the optimized time scale which

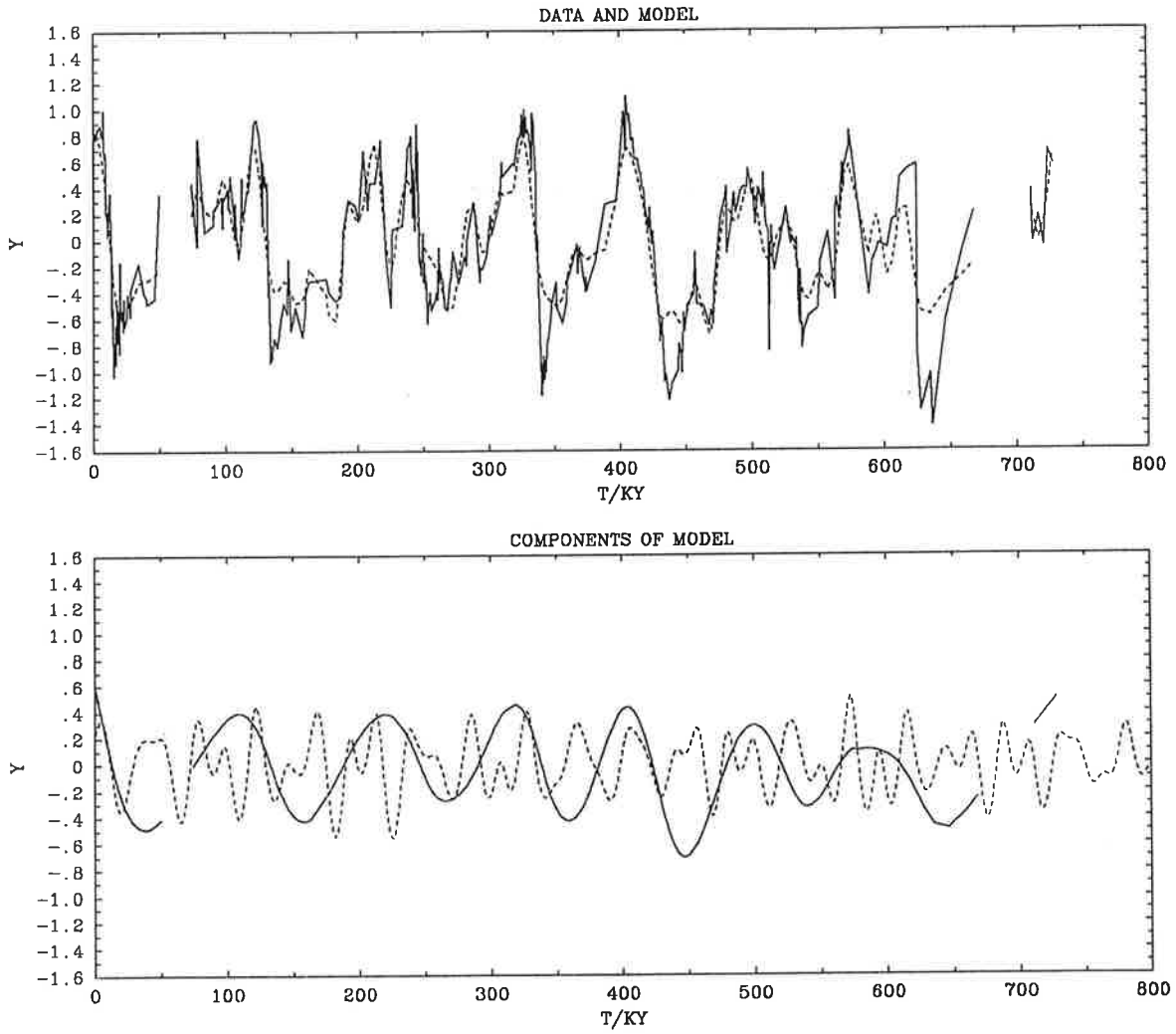

Figure 7: Core ODP 658, SPECMAP age-depth relation. *Top:* The δ^{18}O variation (solid line) and the model (dashed line). *Bottom:* The two components $\bar{y}$ (solid line) and $y_{\odot}$ (dashed line) of the model.

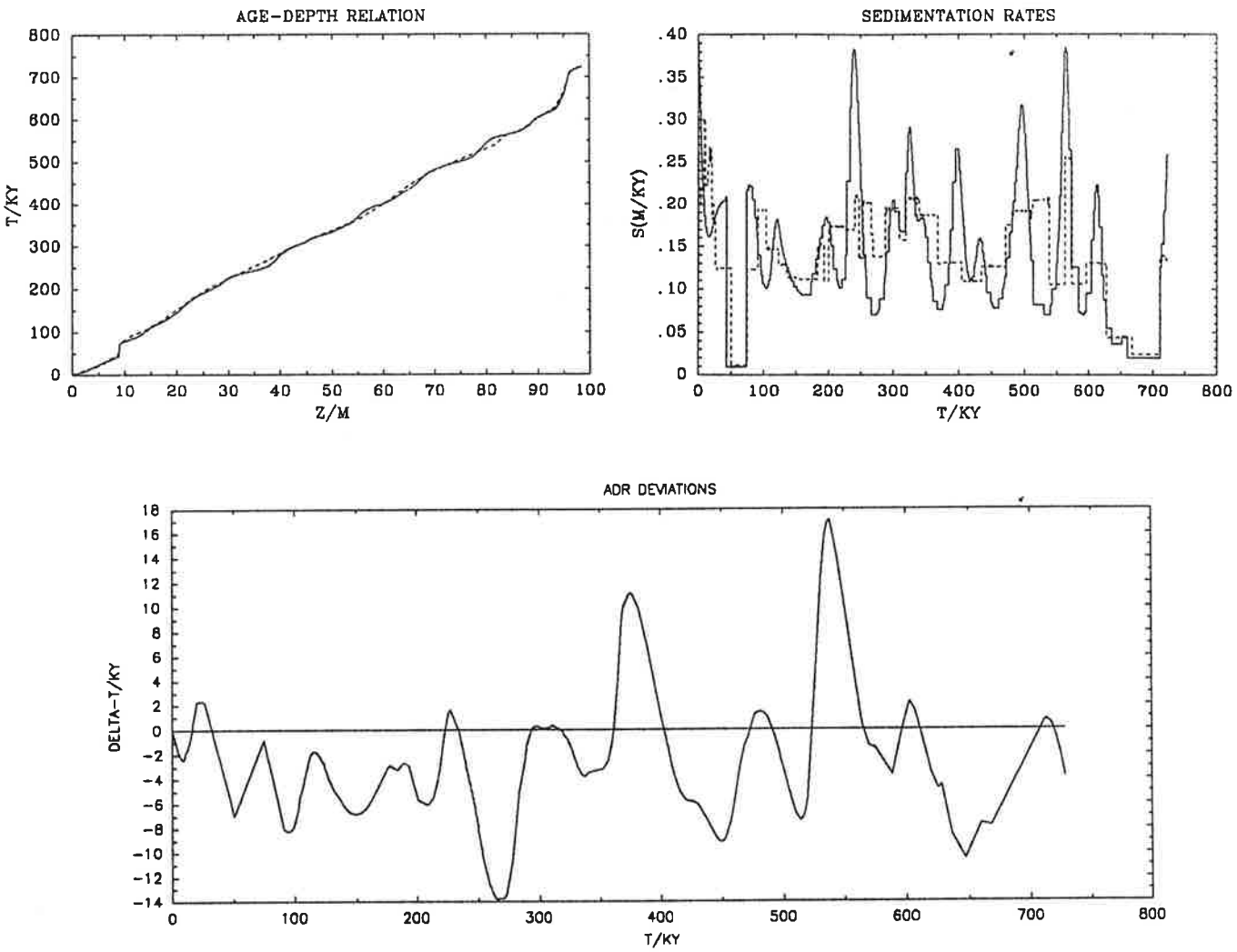

Figure 8: Core ODP 658: *Top left:* The initial (dashed) and optimized (solid) age-depth relation. *Top right:* The initial (dashed) and optimized (solid) sedimentation rate. *Bottom:* The difference of the optimized and the initial age-depth relation. The mean deviation is 6.2 ky.

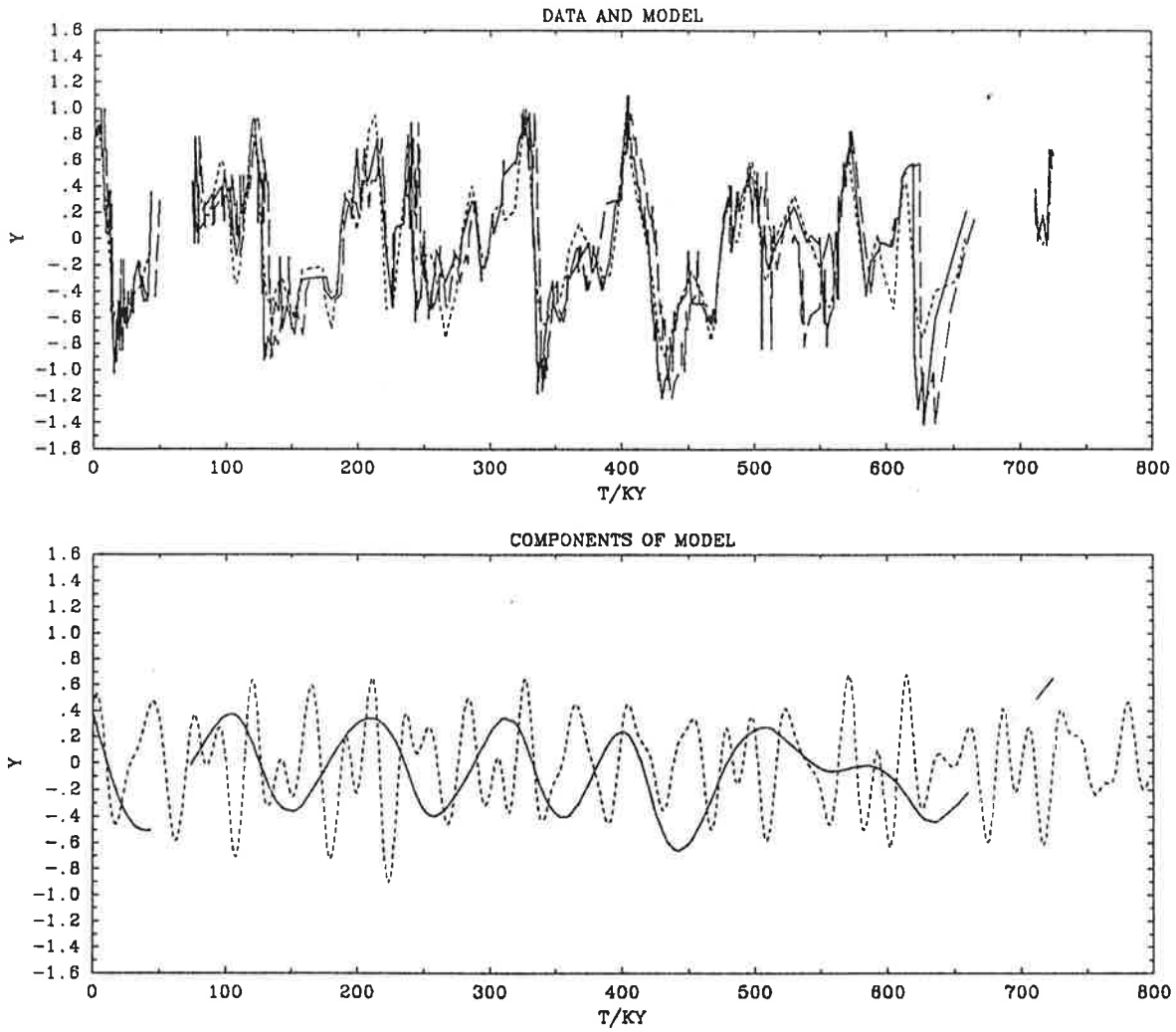

Figure 9: Core ODP 658. *Top:* The δ^{18}O variation in the initial (long dashed) and in the optimized time scale (solid line), and the model for the optimized time scale (short dashed). *Bottom:* The two components $\bar{y}$ (solid line) and $y_{\odot}$ (dashed line) of the model.

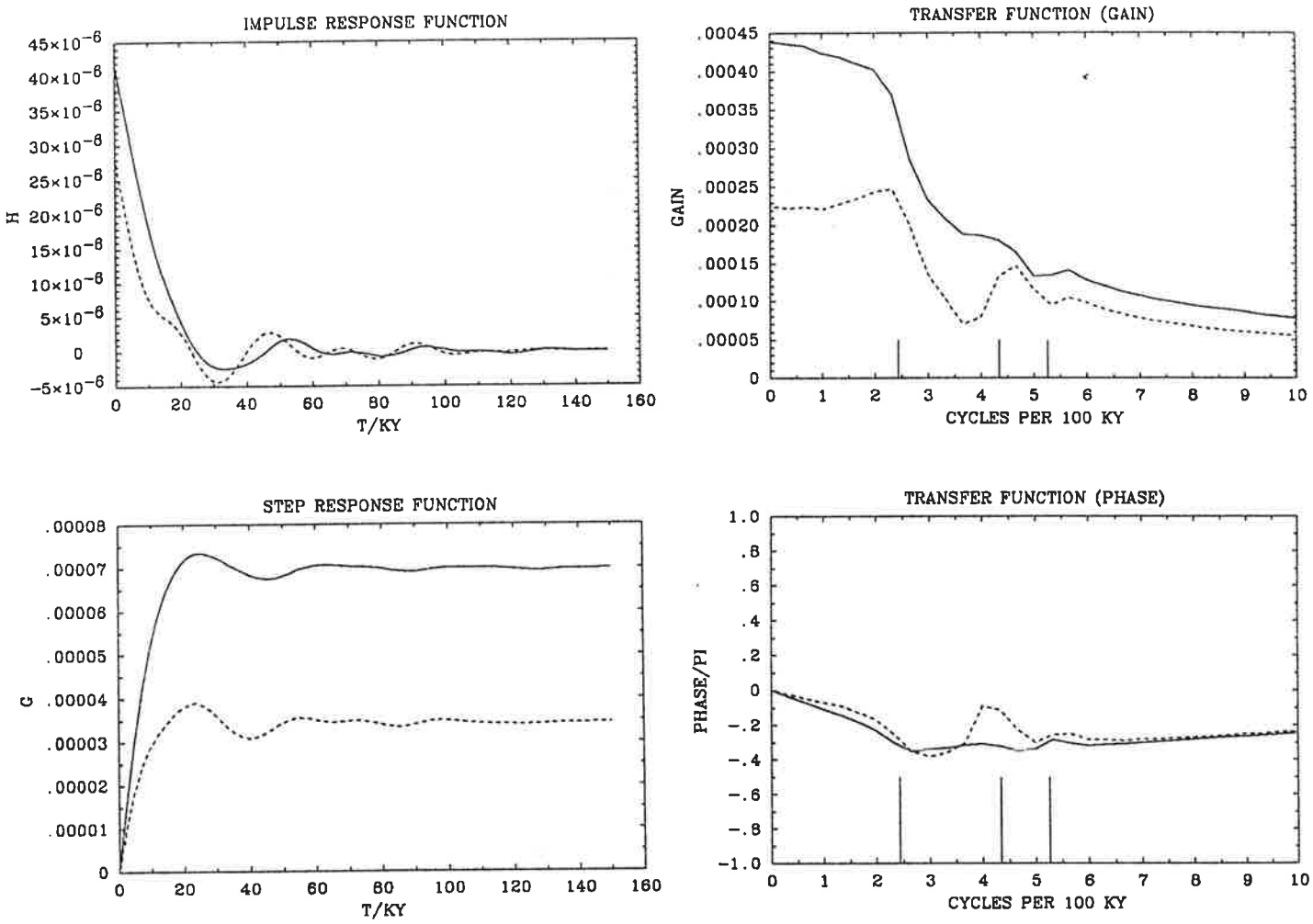

Figure 10: Core ODP 658: The impulse response function h (upper left), the step response function g (lower left), and gain (upper right) and phase (lower right) of the transfer function for the initial (dashed line) and the optimized (solid line) age-depth relation. Vertical lines indicate the astronomical frequencies (41, 23, and 19 ky).

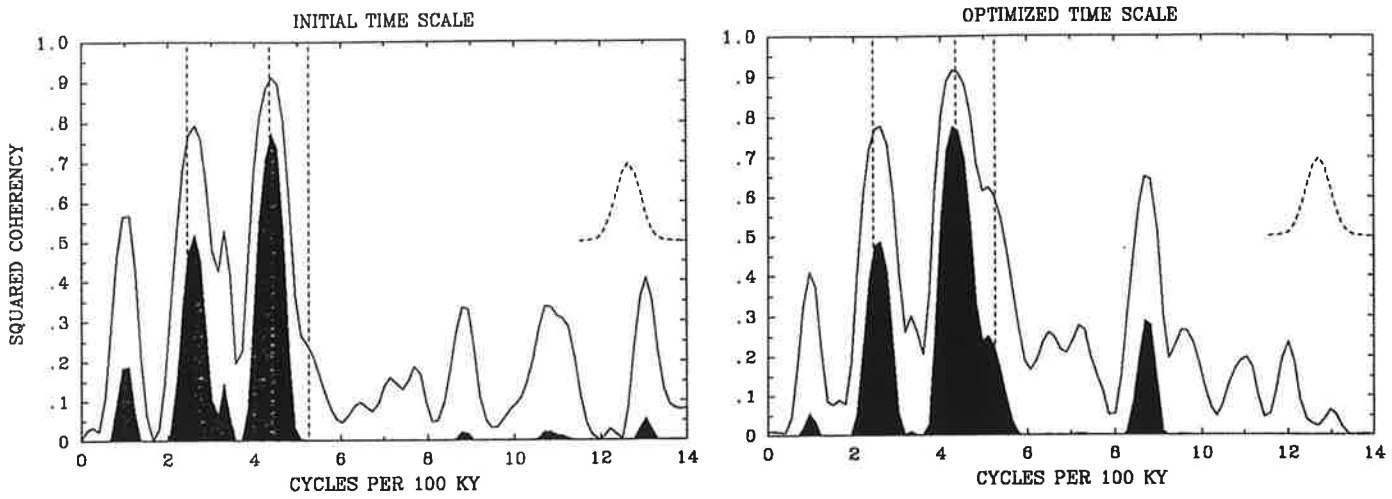

Figure 11: Core ODP 658: Squared coherency between insolation and $\delta^{18}O$ data in the initial (left) and the optimized time scale (right). Shaded regions denote the lower 95 per cent confidence limits. Vertical dashed lines indicate the astronomical frequencies (41, 23, and 19 ky). Dashed curves at the right margin display the spectral window.

is due to a large increase of the variance explained by $y_\odot$ and a small decrease of the variance explained by $\bar{y}$, see table 2.

An examination of the squared coherency between the solar insolation and the $\delta^{18}O$ record before and after the time scale optimization, see Fig. 11, shows, that the coherency at 41 and 23 ky remains almost unaltered, while the coherency at 19 ky is increased from 25 to 60 per cent. Therefore—like for the Meteor core 13519—the linear correlation between solar insolation and $\delta^{18}O$ record is significantly increased by the optimization procedure.

3.3 Sensitivity tests

3.3.1 The parameters of the response model estimation

Into the calculation of the response model enter the three parameters λ_1, λ_2, and μ, which control the smoothness of the impulse response funcion h, the vanishing of h with increasing time, and the smoothness of the residual low-frequency variation $\bar{y}$, compare Eq. (7). The values of the parameters describing the details of the discretisation have no effect as long as they are chosen properly.[8]

For testing the sensitivity of the solution we change every parameter individually by the factors 0.1 and 10 and calculate the corresponding age-depth relation for the core ODP 658. The mean deviation between these age-depth relations and the one with the parameter choice used in section 3.2 is shown in Tab. 1.

The strongest influence is due to the parameter μ, and this is the one which can be determined most accurately. It is set to the smallest possible value that does not allow $\bar{y}$ to contain any significant power in the astronomical frequency bands. This can be

[8]The number m of points of the discrete representation of h has to be choosen so that the smallest features in h are well resolved. The maximum time coordinate u_m must be large enough to contain all significant non-zero values of h.

	×0.1	×10
λ_1	0.40 ky	0.56 ky
λ_2	2.81 ky	2.54 ky
μ	3.99 ky	6.31 ky

Table1: The mean deviation of the age-depth relation, corresponding to changes of the parameters in the left column by the factor in the heading.

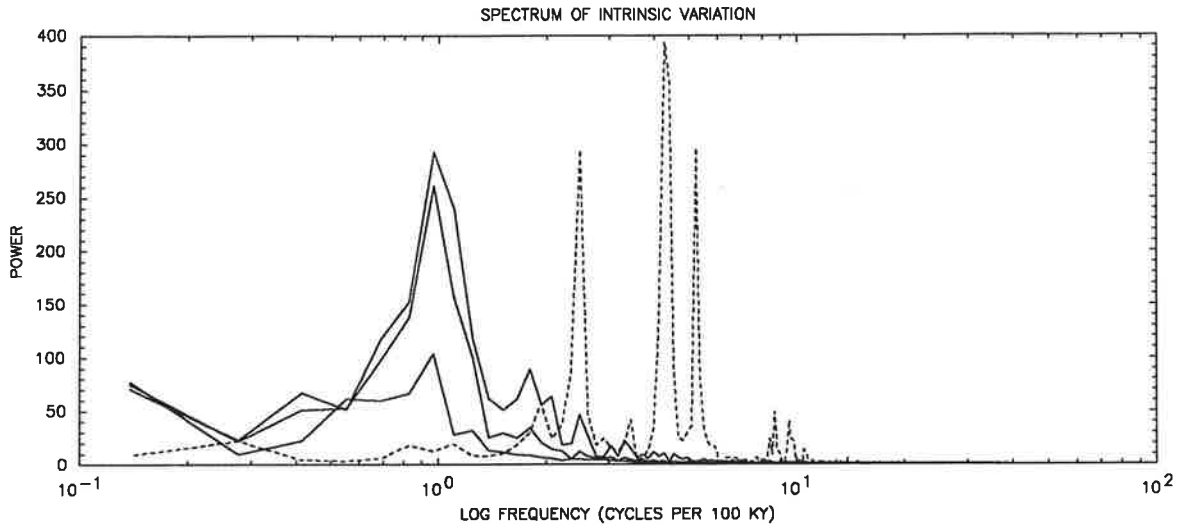

Figure 12: The power spectra of the low-frequency component $\bar{y}$ (solid) for three values of μ differing by a factor 10, the highest peak corresponding to the lowest μ, and the spectrum of the solar insolation (dashed).

achieved by examination of the power spectrum of the intrinsic low frequency component, see Fig. 12. The spectrum with the highest peak—corresponding to the lowest value of μ—still has some power in the 41 ky band. Icreasing μ by a factor 10 supresses this portion without significant impact on the 100 ky band. Repeated increase by a factor 10 drastically reduces the power at 100 ky. Therefore the middle value is obviously preferable.

The experiments with parameters λ_1 and λ_2 changed by factors 0.1 and 10 cover the range throughout which a to some extend reasonable impulse response function is obtained. The stronger dependence on λ_2 is due to the fact that this parameter influences the time scale of the damping of the impulse response function. Given some limits on this time scale, the reasonable range for λ_2 could considerably be narrowed.

3.3.2 The parameters of the time scale optimization

The optimization of the age-depth relation depends on the parameter λ, which controls the smoothness of $\tau(z)$, and on the initial age-depth relation.

Changes of the parameter λ do in fact only influence the smoothness of the sedimentation rates. Solutions with higher λ are like smoothed versions of solutions with lower λ. The determination of this parameter therefore depends on how much variation in the sedimentation rates we are ready to accept.

To examine the dependence of the solution on the initial time scale, we use core ODP 658. We take the initial age-depth relations used in the calculations of section 3.2 and

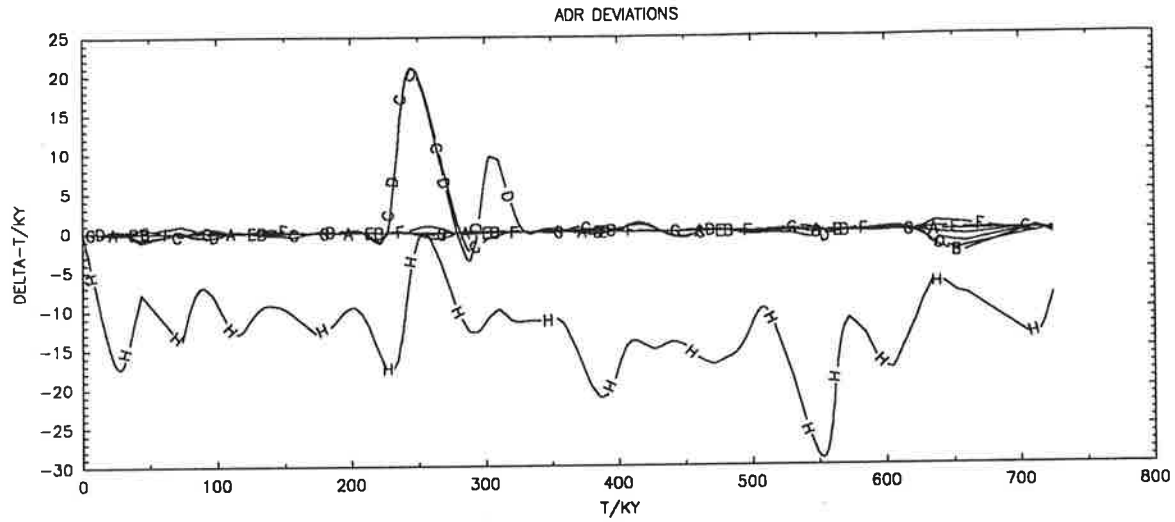

Figure 13: The deviations of the age-depth relations resulting from an initial time scale implying an error function with $e_{max} = 0$ (A), 10 ky (B), 15 ky (C), 20 ky(D), -10 ky (E), -20 ky (F), -25 ky (G), and -30 ky (H).

add a linear error function which vanishes for the present and reaches its maximum value e_{max} at the bottom of the core. We perform calculations using for e_{max} the values -30, -25, -20, -10, 10, 15, and 20 ky. The initial time scales with $e_{max} = -25 \ldots 10$ ky yield the same age-depth relation as the normal run ($e_{max} = 0$). For 15 and 20 ky we obtain partly different time scales, but almost the same response model, while the value -30 ky leads to a completely different time scale and a qualitative different response function (i. e. increasing ice-volume for larger solar insolation). The various resulting age-depth relations are compared in Fig. 13.

The solution does not depend on the iteration damping parameter γ, compare Eq. (19), as long as the damping is strong enough to prevent extensive oscillations of the age-depth relation during the iteration.

4 Discussion

The main difficulty in the critical examination of the resultant chronologies is that there are very few independent age determinations. The Isotopic stage boundary 6.0 was radiometrically dated to have an age of 127 $\pm$ 6 ky, which is consistant with the value 126.5 ky given by our results. The most reliable fix point beyond 300 ky is propably the Brunhes-Matuyama-Boundary, which is generally believed to have an age of about 730 ky, see e. g. Mankinen and Dalrymple (1979). This lies well within the range given by our results, which determine the Brunhes-Matuyama-Boundary to be between 729 and 732 ky, see section 3.1.

Passable agreement with the few independent age determinations was also achieved by various other Quaternary chronologies, the most widly used of which is the SPECMAP time scale, but we did not use the known ages in the optimization, and so their reproduction is a confirmation of the results.

A main advantage of the method presented in this paper is that every core is adapted to the solar insolation corresponding to its individual resolution, whereas the SPECMAP

Core	Meteor 13519		ODP 658	
Chronology	SPECMAP	Optimized	SPECMAP	Optimized
Solar insolation	8%	29%	29%	47%
Low-frequency comp.	52%	42%	53%	40%
Total	61%	70%	75%	82%

Table2: The data variance explained by the two model components.

dating is limited to the correlation with an averaged, smoothed standard stack.

In table 2 the percentages of data variance explained by the models are shown. The absolut values should not be taken too seriously, because they depend on the parameters λ, λ_1, λ_2, and μ. Reduction of one or more of these would yield an increased explained variance—at the cost of some more structure in the model functions and the sedimentation rates that does not seem reasonable. The purpose of the specification of the explained variance is the comparism of the different cores and the different chronologies. For both cores the optimization leads to considerably increased explained variances compared with the SPECMAP time scale. The core ODP 658 seemed to be more proper to a decription by our model than the Meteor core 13519. This may possibly in part be due to the fact, that the former's data were taken from a *benthic* species while the later's were taken from a *planktonic* spezies, which might be more influenced by local effects.

In our calculations we assume the characteristics of the response of the ice volume to changes in the solar insolation—defined by the impulse response function—to be constant over the observed time. Recent investigations of the validity of this assumption [21] showed, that differences in the amlitudes of the response can be explained by varying response times[9], i. e. varying impulse response function. The effects on an orbitally tuned chronology are estimated to result in deviations smaller than 3.5 ky.

It is quite interesting to compare the low-frequency components $\bar{y}$ of the model $\delta^{18}O$ variations for the two cores with the eccentricity of the earth orbit, see Fig. 14. The strong correlation suggests that the eccentricity should be implicated directly in the construction of a model, allthough no physical mechanism for the connection of eccentricity and global ice volume is known yet.

The main problem of the presented method is the sensibility to changes in the initial age-depth relation. In most cases this propably prohibits the use of a simple linear time scale as initial chronology. One has to supply a time scale with an error of not much more than about 10 ky, which could for instance be obtained by correlation with the SPECMAP standard stack. Possibly an extented version of the presented method, which could be applied to many cores simultaniously, will be more stable to changes in the initial chronology.

[9]The observed differences can also directly be explained by changes of the *amplitude* of the response, rather than the response *time*, which would not yield the estimated effect on orbitally tuned chronologies.

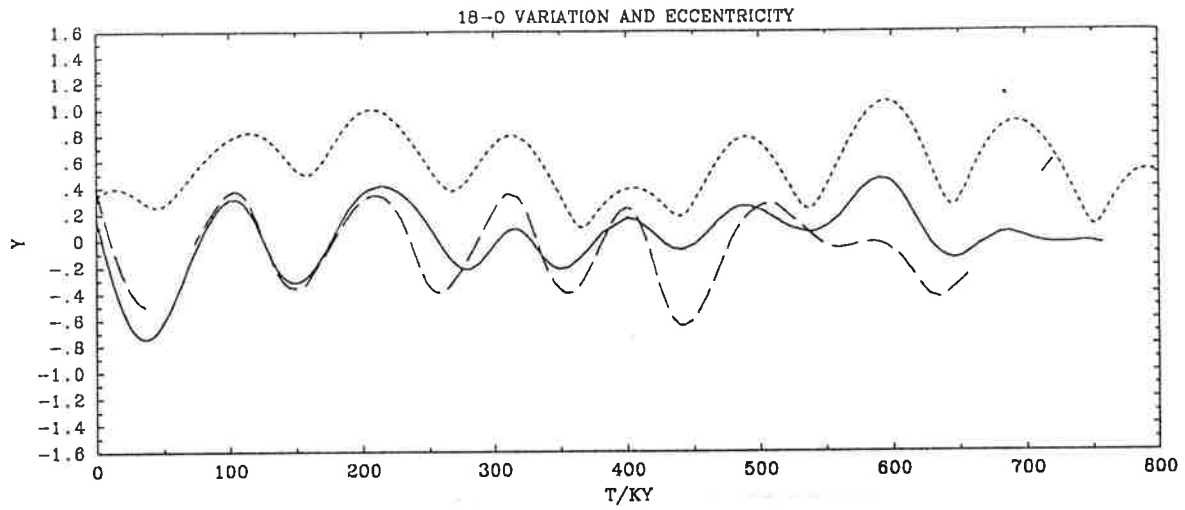

Figure 14: The low-frequency component $\bar{y}$ of the model $\delta^{18}O$ variation for the Meteor core 13519 (solid line) and the core ODP 658 (long dashed), compared with the eccentricity of the earth orbit (short dashed, conveniently scaled).

A Appendix

A.1 Unconstrained calculation of the transfer function

In the following we describe the calculation of the transfer function for uneven spaced $\delta^{18}O$ data $(t_i, y_i)_{i=1,\ldots,n}$. The variation of the solar insolation is given as continous function $x(t)$ [1]. Let Δt be the discretization time step and N the number of points. The autocorrelation function of $x(t)$ is then given by

$$r_{xx}(i\Delta t) = \frac{1}{N}\sum_{j=1}^{N} x(j\Delta t)x((j-i)\Delta t). \tag{20}$$

The cross correlation function of $x(t)$ and $y(t)$ is

$$r_{xy}(i\Delta t) = \frac{1}{n}\sum_{j=1}^{n} y_j x(t_j - i\Delta t). \tag{21}$$

These discrete representations of r_{xx} and r_{xy} are equally spaced, so their Fourier transforms R_{xx} and R_{xy}, respectively, can be calculated using standard spectral analysis. The transfer function is given by

$$H = \frac{R_{xy}}{R_{xx}}. \tag{22}$$

It is of course only defined for frequencies at which R_{xx} is significantly different from zero.

A.2 The calculation of the convolution matrix X

The portion of the $\delta^{18}O$ variation due to linear impact of the solar insolation is given by

$$y_{\odot}(t) = \int_0^{\infty} h(u)x(t-u)du. \tag{23}$$

If we assume the impulse response function h to be given by a polygonian $(u_j, h_j)_{j=1,\ldots,m}$, i. e.

$$h(u) = h_{j-1} + h'_j(u - u_{j-1}) \qquad \text{for } u_{j-1} < u \leq u_j \tag{24}$$

with

$$h'_j = \frac{h_j - h_{j-1}}{u_j - u_{j-1}}, \tag{25}$$

we obtain

$$y_\odot(t) = \sum_{j=2}^{m} \int_{u_{j-1}}^{u_j} [h_{j-1} + h'_j(u - u_{j-1})] x(t-u) du, \tag{26}$$

or

$$y_\odot(t) = \sum_{j=2}^{m} y_j(t), \tag{27}$$

with

$$\begin{aligned} y_j(t) &:= \int_{u_{j-1}}^{u_j} [h_{j-1} + h'_j(u - u_{j-1})] x(t-u) du \\ &= (h_{j-1} - h'_j u_{j-1}) \int_{u_{j-1}}^{u_j} x(t-u) du + h'_j \int_{u_{j-1}}^{u_j} u x(t-u) du. \end{aligned} \tag{28}$$

We assume $x(t-u)$ to be linear between $t - u_j$ and $t - u_{j-1}$. Introducing

$$\begin{aligned} x_j(t) &:= x(t - u_j), \\ x'_j(t) &:= \frac{x_j(t) - x_{j-1}(t)}{u_j - u_{j-1}} \end{aligned} \tag{29}$$

we then obtain

$$x(t-u) = x_{j-1}(t) + x'_j(t)(u - u_{j-1}) \qquad \text{for } u_{j-1} < u \leq u_j. \tag{30}$$

Inserting this in Eq. (28) yields

$$\begin{aligned} y_j(t) &= (h_{j-1} - h'_j u_{j-1}) \int_{u_{j-1}}^{u_j} x_{j-1}(t) + x'_j(t)(u - u_{j-1}) du + \\ &\quad + h'_j \int_{u_{j-1}}^{u_j} u x_{j-1}(t) + u x'_j(t)(u - u_{j-1}) du \\ &= (h_{j-1} - h'_j u_{j-1}) \left[(x_{j-1}(t) - x'_j(t) u_{j-1})(u_j - u_{j-1}) + \frac{1}{2} x'_j(t)(u_j^2 - u_{j-1}^2) \right] + \\ &\quad + h'_j \left[\frac{1}{2} (x_{j-1}(t) - x'_j(t) u_{j-1})(u_j^2 - u_{j-1}^2) + \frac{1}{3} x'_j(t)(u_j^3 - u_{j-1}^3) \right]. \end{aligned} \tag{31}$$

Now we define

$$\begin{aligned} A_j &:= -\frac{u_{j-1}}{u_j - u_{j-1}}, \\ B_{ij} &:= (x_{j-1}(t_i) - x'_j(t_i) u_{j-1})(u_j - u_{j-1}) + \frac{1}{2} x'_j(t_i)(u_j^2 - u_{j-1}^2), \end{aligned} \tag{32}$$

$$C_{ij} := -\frac{\frac{1}{2}(x_{j-1}(t_i) - x'_j(t_i) u_{j-1})(u_j^2 - u_{j-1}^2) + \frac{1}{3} x'_j(t_i)(u_j^3 - u_{j-1}^3)}{u_j - u_{j-1}}. \tag{33}$$

Taking into account the definition of h'_j, Eq. (25), we obtain

$$\begin{aligned} y_j(t_i) &= B_{ij}[h_{j-1} + A_j(h_j - h_{j-1})] - C_{ij}(h_j - h_{j-1}) \\ &= B_{ij}h_{j-1} + A_jB_{ij}h_j - A_jB_{ij}h_{j-1} - C_{ij}h_j + C_{ij}h_{j-1} \\ &= (A_jB_{ij} - C_{ij})h_j + (B_{ij} + C_{ij} - A_jB_{ij})h_{j-1}. \end{aligned} \tag{34}$$

If furthermore

$$\begin{aligned} D_{ij} &:= A_jB_{ij} - C_{ij}, \\ E_{ij} &:= B_{ij} + C_{ij} - A_jB_{ij}, \end{aligned} \tag{35}$$

we get

$$y_j(t_i) = D_{ij}h_j + E_{ij}h_{j-1}. \tag{36}$$

Inserting this into Eq. (27) leads to

$$y_\odot(t_i) = \sum_{j=1}^{m} D_{ij}h_j + E_{ij}h_{j-1}, \tag{37}$$

with $h_0 := 0$. If we set $E_{i,m+1} := 0$ we obtain

$$y_\odot(t_i) = \sum_{j=1}^{m}(D_{ij} + E_{i,j+1})h_j. \tag{38}$$

Therefore we see that

$$X_{ij} := D_{ij} + E_{i,j+1} \tag{39}$$

is the convolution matrix, since the δ^{18}O variation due to linear impact of the solar insolation is given by

$$y_\odot(t_i) = \sum_{j=1}^{m} X_{ij}h_j. \tag{40}$$

A.3 The smoothing and damping matrizes

Let $(t_j, y_j)_{j=1,\ldots,n}$ be the discrete representation of a function $y(t)$ and $\mathcal{F}(y)$ the norm of its second derivative. Then the smoothing matrix F is defined by

$$\frac{1}{2}\frac{\partial}{\partial y_i}\mathcal{F}(y) = \sum_{j=1}^{n} F_{ij}y_j. \tag{41}$$

If the time coordinates t_j are equally spaced with distance Δ, the smoothing matrix $(F_1)_{ij}$ is given by [4][10]

$$F_1 = \frac{1}{\Delta^3}\begin{pmatrix} 1 & -2 & 1 & & & & 0 \\ -2 & 5 & -4 & 1 & & & \\ 1 & -4 & 6 & -4 & 1 & & \\ & \ddots & \ddots & \ddots & \ddots & \ddots & \\ & & 1 & -4 & 6 & -4 & 1 \\ & & & 1 & -4 & 5 & -2 \\ 0 & & & & 1 & -2 & 1 \end{pmatrix}. \tag{42}$$

[10]The factor $1/\Delta^3$ is frequently omited, which implies that it is incorporated in the smoothing parameter, compare Eqs. (7,10).

If the time coordinates t_j are *not* equally spaced, the calculation of the smoothing matrix is a little bit more complicate. The second derivative at the point t_j is given by

$$\begin{aligned} y_j'' &= \frac{\frac{y_{j+1}-y_j}{t_{j+1}-t_j} - \frac{y_j-y_{j-1}}{t_j-t_{j-1}}}{\frac{1}{2}(t_{j+1}-t_{j-1})} \\ &= \frac{2}{(t_{j+1}-t_j)(t_{j+1}-t_{j-1})}\ y_{j+1} + \\ &\quad + \left(\frac{2}{(t_{j+1}-t_j)(t_{j+1}-t_{j-1})} + \frac{2}{(t_j-t_{j-1})(t_{j+1}-t_{j-1})}\right)\ y_j + \\ &\quad + \frac{2}{(t_j-t_{j-1})(t_{j+1}-t_{j-1})}\ y_{j-1}. \end{aligned} \tag{43}$$

Introducing

$$\begin{aligned} \alpha_j &:= \frac{\sqrt{2}}{(t_{j+1}-t_j)\sqrt{t_{j+1}-t_{j-1}}}, \\ \beta_j &:= \frac{\sqrt{2}}{(t_j-t_{j-1})\sqrt{t_{j+1}-t_{j-1}}}, \\ \gamma_j &:= \alpha_j + \beta_j, \end{aligned} \tag{44}$$

we obtain for the norm of the second derivative of y

$$\begin{aligned} \mathcal{F}(y) &= \sum_{j=2}^{n-1}(y_j'')^2 \cdot \frac{1}{2}(t_{j+1}-t_{j-1}) \\ &= \sum_{j=2}^{n-1}[\alpha_j y_{j+1} - \gamma_j y_j + \beta_j y_{j-1}]^2 \\ &= \sum_{j=2}^{n-1} \alpha_j^2 y_{j+1}^2 + \gamma_j^2 y_j^2 + \beta_j^2 y_{j-1}^2 + \\ &\quad + 2\alpha_j\beta_j y_{j+1}y_{j-1} - 2\alpha_j\gamma_j y_{j+1}y_j - 2\beta_j\gamma_j y_j y_{j-1}. \end{aligned} \tag{45}$$

Derivation of $\mathcal{F}(y)$ with respect to y_i yields

$$\begin{aligned} \frac{1}{2}\frac{\partial}{\partial y_i}\mathcal{F}(y) &= [\alpha_{i-1}^2 y_i + \alpha_{i-1}\beta_{i-1}y_{i-2} - \alpha_{i-1}\gamma_{i-1}y_{i-1}](1-\delta_{i,1})(1-\delta_{i,2}) + \\ &\quad + [\gamma_i^2 y_i - \alpha_i\gamma_i y_{i+1} - \beta_i\gamma_i y_{i-1}](1-\delta_{i,1})(1-\delta_{i,n}) + \\ &\quad + [\beta_{i+1}^2 y_i + \alpha_{i+1}\beta_{i+1}y_{i+2} - \beta_{i+1}\gamma_{i+1}y_{i+1}](1-\delta_{i,n-1})(1-\delta_{i,n}), \end{aligned} \tag{46}$$

where $\delta_{i,j}$ denotes the Kronecker Delta. The smoothing matrix $(F_2)_{ij}$ is then given by

$$F_2 = \begin{pmatrix} \beta_2^2 & -\beta_2\gamma_2 & \alpha_2\beta_2 & & & & & 0 \\ -\beta_2\gamma_2 & \gamma_2^2+\beta_3^2 & \begin{pmatrix} -\alpha_2\gamma_2 \\ -\beta_3\gamma_3 \end{pmatrix} & \alpha_3\beta_3 & & & & \\ & \ddots & \ddots & \ddots & \ddots & & & \\ & & & f_{ij} & & & & \\ & & \ddots & \ddots & \ddots & \ddots & & \\ & & & \alpha_{n-2}\beta_{n-2} & \begin{pmatrix} -\alpha_{n-2}\gamma_{n-2} \\ -\beta_{n-1}\gamma_{n-1} \end{pmatrix} & \alpha_{n-2}^2\gamma_{n-1}^2 & -\alpha_{n-1}\gamma_{n-1} & \\ 0 & & & & \alpha_{n-1}\beta_{n-1} & -\alpha_{n-1}\gamma_{n-1} & \alpha_{n-1}^2 & \end{pmatrix}, \tag{47}$$

where f_{ij} is defined for $i = 3, \ldots, n-2$ by

$$f_{ij} = \begin{cases} \alpha_{i-1}\beta_{i-1} & \text{for } j = i-2 \\ -\alpha_{i-1}\gamma_{i-1} - \beta_i\gamma_i & \text{for } j = i-1 \\ \alpha_{i-1}^2 + \gamma_i^2 + \beta_{i+1}^2 & \text{for } j = i \\ -\alpha_i\gamma_i - \beta_{i+1}\gamma_{i+1} & \text{for } j = i+1 \\ \alpha_{i+1}\beta_{i+1} & \text{for } j = i+2 \\ 0 & \text{otherwise} \end{cases} \tag{48}$$

Let the mapping $\mathcal{G}$ be given by Eq. (9) and $(u_j, h_j)_{j=1,\ldots,n}$ be an equally spaced representation of the function $h(u)$ with step width Δ. Then is

$$\begin{aligned} \frac{1}{2}\frac{\partial}{\partial h_i}\mathcal{G}(h) &= \frac{1}{2}\frac{\partial}{\partial h_i}\sum_{j=1}^{n} u_j^2 h_j^2 \Delta \\ &= \Delta u_i^2 h_i. \end{aligned} \tag{49}$$

Therefore the matrix G, compare Eq. (10), is given by

$$G_{ij} = \begin{cases} \Delta u_i^2 & \text{for } i = j \\ 0 & \text{otherwise.} \end{cases} \tag{50}$$

A.4 The linear equation system for impulse response function and low-frequency component

Derivation of Eq. (7) with respect to h_k yields

$$\begin{aligned} & \frac{\partial}{\partial h_k}\left[\sum_{i=1}^{n}\left(y_i - \bar{y}_i - \sum_{j=1}^{m} X_{ij}h_j\right)^2 + \lambda_1\mathcal{F}(h) + \lambda_2\mathcal{G}(h) + \mu\mathcal{F}(\bar{y})\right] = 0 \\ \iff & \sum_{i=1}^{n} 2X_{ik}\left(\sum_{j=1}^{m} X_{ij}h_j + \bar{y}_i - y_i\right) + 2\lambda_1\sum_{j=1}^{m}(F_1)_{kj}h_j + 2\lambda_2\sum_{j=1}^{m} G_{kj}h_j = 0 \\ \iff & 2(X^TXh)_k + 2(X^T\bar{y})_k - 2(X^Ty)_k + 2\lambda_1(F_1h)_k + 2\lambda_2(Gh)_k = 0 \\ \iff & (X^TXh)_k + \lambda_1(F_1h)_k + \lambda_2(Gh)_k + (X^T\bar{y})_k = (X^Ty)_k, \end{aligned} \tag{51}$$

where F_1 and G are given by Eqs. (42,50). By assembling the derivatives for all $k = 1, \ldots, m$ we obtain Eq. (10).

Now we derive Eq. (7) with respect to $\bar{y}_l$:

$$\begin{aligned} & \frac{\partial}{\partial \bar{y}_l}\left[\sum_{i=1}^{n}\left(y_i - \bar{y}_i - \sum_{j=1}^{m} X_{ij}h_j\right)^2 + \lambda_1\mathcal{F}(h) + \lambda_2\mathcal{G}(h) + \mu\mathcal{F}(\bar{y})\right] = 0 \\ \iff & 2\left(\sum_{j=1}^{m} X_{lj}h_j + \bar{y}_l - y_l\right) + 2\mu\sum_{j=1}^{m}(F_2)_{lj}\bar{y}_j = 0 \\ \iff & 2(Xh)_l + 2\bar{y}_l - 2y_l + 2\mu(F_2\bar{y})_l \\ \iff & (Xh)_l + \bar{y}_l + \mu(F_2\bar{y})_l = y_l, \end{aligned} \tag{52}$$

where F_2 is given by Eqs. (47,48). By assembling the derivatives for all $l = 1, \ldots, n$ we obtain Eq. (11).

A.5 The derivatives of the target function for the optimization of the age-depth relation

The age-depth relation is choosen to minimize

$$\varepsilon(r) = \sum_{i=1}^{n} [\Delta y_i - y_\odot(\tau(z_i))]^2 + \lambda \mathcal{F}(s). \tag{53}$$

The vector Δy is defined by Eq. (12). The function $y_\odot(t)$ can be obtained by linear interpolation of the points $(\tilde{t}_k, (\tilde{X}h)_k)$ i. e.

$$y_\odot(t) = (\tilde{X}h)_{k-1} + \frac{(\tilde{X}h)_k - (\tilde{X}h)_{k-1}}{\tilde{t}_k - \tilde{t}_{k-1}}(t - \tilde{t}_{k-1}) \qquad \text{for } \tilde{t}_{k-1} < t \leq \tilde{t}_k, \tag{54}$$

where $\tilde{t}_k$ are time coordinates covering the possible range of the chronology with a spacing narrow enough to resolve the variation of the solar insolation and $\tilde{X}$ is the convolution matrix calculated with these $\tilde{t}_k$.[11]

The derivatives of ε are

$$\frac{\partial \varepsilon}{\partial r_j} = \sum_{i=1}^{n} \left[-2[\Delta y - y_\odot(\tau(z_i))] \frac{\partial y_\odot(\tau(z_i))}{\partial r_j} + 2\lambda (F_2)_{ij} \right], \tag{55}$$

with F_2 given by Eq. (47). At a given point r the corresponding age-depth relation $\tau(z)$ is known from Eq. (16) and the derivative of $y_\odot(\tau(z_i))$ is given by

$$\begin{aligned} \frac{\partial y_\odot(\tau(z_i))}{\partial r_j} &= \frac{\partial y_\odot}{\partial t}(\tau(z_i)) \frac{\partial \tau}{\partial r_j} \\ &= \frac{(\tilde{X}h)_k - (\tilde{X}h)_{k-1}}{\tilde{t}_k - \tilde{t}_{k-1}} Z_{ij} \qquad \text{for } \tilde{t}_{k-1} < \tau(z_i) \leq \tilde{t}_k, \end{aligned} \tag{56}$$

with

$$Z_{ij} = \begin{cases} z_j - z_{j-1} & \text{if } i \geq j \\ 0 & \text{otherwise.} \end{cases} \tag{57}$$

References

[1] A. L. Berger: 1977, "Long term variations of the Earth's orbital elements", *Celestial Mechanics* **15,** 53–74

[2] Ulrich Bleil, Volkhard Spiess, Norbert Weinreich: 1984, "A hiatus in early Quaternary sediments documented in the magnetostratigraphic record of "Meteor" core 13519 from the eastern equatorial Atlantic", *"Meteor" Forschungsergebnisse* Reihe C — No. 38, 1–7

[3] R. S. Bradley: 1985, *Quaternary Paleoclimatology* (Boston: Unwin Hyman)

[4] Jan J. D. Craig, John C. Brown: 1986, *Inverse Problems in Astronomy* (Bristol: Adam Hilger Ltd)

[11] We recommend not to use the time coordinates t_i of the $\delta^{18}O$ measurements and the corresponding matrix X. The spacing may—at least partially—be much too wide, which could hinder convergence.

[5] James Croll: 1864, "Climate and time", *Philos. Mag.* **28,** 121

[6] Daniel Fischer: 1990, "Die Bahnen der Planeten: ein chaotisches system?", *Sterne und Weltraum* **1,** 28–31

[7] Joel N. Franklin: 1970, "Well-Posed Stochastik Extensions of Ill-Posed linear Problems", *Journal of Mathematical Analysis and Applications* **31,** 682

[8] Hays, J. D., Imbrie, J., Shackleton, N. J.: 1976, "Variations in the earth's orbit: pacemaker of the ice ages", *Science* **194,** 1121–1132

[9] K. Herterich, M. Sarnthein: 1984, "Brunhes time scale: Tuning by rates of calcium-carbonate dissolution and cross spectral analysis with solar insolation", *Milankovič and Climate, Part I,* ed. A. Berger, J. Imbrie, J. Hays, G. Kukla, B. Saltzman (Dortrecht, Boston, Lancaster: D. Reidel Publishing Company), 447–466

[10] Klaus Herterich: 1987, "Die astronomische Theorie der Eiszeiten", *Sterne und Weltraum* **5,** 272–276

[11] Klaus Herterich: 1988, "Extracting the parameter of simple climate models by inverse modeling of the deep-sae core climatic record", Max-Planck-Institut für Meteorologie, Report 23

[12] John Imbrie, John Z. Imbrie: 1980, "Modeling the Climatic Response to Orbital Variations", *Science* **207**, 943–953

[13] John Imbrie, Katharine Palmer Imbrie: 1981, *Die Eiszeiten* (Düsseldorf, Wien: Econ Verlag GmbH)

[14] J. Imbrie, J. D. Hays, D. G. Martinson, A. McIntyre, A. C. Mix, J. J. Morley, N. G. Pisias, W. L. Prell, N. J. Shackleton: 1984, "The orbital theory of Pleistocene climate: Support from a revised chronology of the marine δ^{18}O record", *Milankovič and Climate, Part I,* ed. A. Berger, J. Imbrie, J. Hays, G. Kukla, B. Saltzman (Dortrecht, Boston, Lancaster: D. Reidel Publishing Company), 269–306

[15] Gwilym M. Jenkins, Donald G. Watts: 1968, *Spectral analysis and its applications* (San Francisco, Cambridge, London, Amsterdam: Holden-Day)

[16] J. Laskar: 1988, "Secular evolution of the solar system over 10 million years", *Astronomy and Astrophysics* **198,** 341–362

[17] J. Laskar: 1989, "A numerical experiment on the chaotic behaviour of the solar system", *Nature* **338,** 237–238

[18] Alfred Karl Louis: 1989, *Inverse und schlecht gestellte Probleme* (Stuttgart: B. G. Teubner)

[19] Edward A. Mankinen, G. Brent Dalrymple: 1979, "Revised Geomagnetic Polarity Time Scale for the Interval 0–5 m.y. B.P.", *Journal of Geophysical Research* **84,** 615–626

[20] Douglas G. Martinson, Nicklas G. Pisias, James D. Hays, John Imbrie, Theodore C. Moore, Jr., Nicholas J. Shackleton: 1987, "Age Dating and the Orbital Theory of the Ice Ages: Development of a High-Resolution 0 to 300,000-Year Chronostratigraphy", *Quaternary Research* **27**, 1–29

[21] Nicklas G. Pisias, Alan C. Mix, Rainer Zahn: 1990, "Nonlinear response in the global climate system: Evidence from benthic oxygen isotope record in core RC13-110", *Paleoceanography* **5**, 147–160

[22] Warren L. Prell, John Imbrie, Douglas G. Martinson, Joseph J. Morley, Nicklas G. Pisias, Nicholas J. Shackleton, Harold F. Streeter: 1986, "Graphic correlation of oxygen isotope stratigraphy: application to the late Quaternary", *Paleoceanography* **1**, 137–162

[23] Barry Saltzman: 1987, "Carbon dioxide and the $\delta^{18}O$ record of late-Quaternary climatic change: a global model", *Climate Dynamics* **1**, 77–85

[24] M. Sarnthein, H. Erlenkeuser, R. von Grafenstein, C. Schröder: 1984, "Stable-isotope stratigraphy for the last 750,000 years: "Meteor" core 13519 from the eastern equatorial Atlantic", *"Meteor" Forschungsergebnisse* Reihe C — No. 38, 9–24

[25] Michael Sarnthein, Ralf Tiedemann: 1990, "Younger Dryas-style cooling events at glacial Terminations I–VI at ODP site 658: Associated Benthic $\delta^{13}C$ anomalies constrain meltwater hypothesis", *Preprint*

[26] Ralf Tiedemann: 1990, "Acht Millionen Jahre Klimageschichte von Nordwest Afrika und Paläo-Ozeanographie des angrenzenden Atlantiks: Hochauflösende Zeitreihen von ODP Sites 658–661", *Ph. D. Thesis,* Universität Kiel

[27] V. F. Turchin, V. P. Kozlov, M. S. Malkevich: 1971, "The use of mathematical-statistics methods in the solution of incorrectly posed problems", *Soviet Physics Uspekhi* **13**, 681